QUANTIFYING PHYSICAL CHARACTERISTICS AND WEATHERING OF BEDROCK IN RELATION TO LANDSCAPE DEVELOPMENT IN THE COLORADO FRONT RANGE

By Alexandra Michelle Horne

A thesis presented to the Faculty of Mount Holyoke College in partial fulfillment of the requirements for the Degree of Bachelors of Arts with Honors

Department of Geology and Geography
Mount Holyoke College
South Hadley, Ma 01075

May, 2012

Advisor: Alan Werner
Committee Members: Alan Werner, Michelle Markley, and Michael Davis
Department Chair: Michelle Markley

ABSTRACT

Bedrock weathering is a fundamental component of critical zone geomorphology that can be influenced by rock strength, fracture spacing, mineralogy, and topoclimate. By quantifying rock strength, we can characterize bedrock weathering across a landscape and interpret its influence on the evolution of local geologic features, such as tors.

This study measured the compressive strength and fracture characteristics of bedrock throughout the Boulder Creek watershed to assess the degree of weathering. Test sites included glacially polished and adjacent weathered alpine bedrock, weathered tors and saprolite in areas of lower elevation, and several highway road exposures. The data collected shows an inversely proportional relationship between depth/degree of weathering and the compressive strength of bedrock. Once bedrock begins to weather, it weakens to an intermediate range of compressive strength, and with increased chemical and physical weathering becomes the weakest local rock measured. At lower elevations, structural anisotropy, microclimate, and regolith removal are the dominant forces governing tor location, size, and differential weathering.

ACKNOWLEDGEMENTS

I would like to thank the KECK Geology Consortium for funding my field work in the Summer of 2011, as well as my advisor, Al Werner, for all of his support and help during this project; David Dethier and Will Ouimet for their input and troubleshooting; Michele Cooke for conversations vital to my understanding of the Schmidt Hammer; the fabulous team I was able to work with in Colorado and without whom I couldn't have collected all of this data: Sarah Beganskas, Neil Shea, and James Winkler; and finally, the students, faculty, and administrators of the Mount Holyoke College Departments of Geology and Geography for their humor, support and troubleshooting.

TABLE of CONTENTS

LIST OF FIGURES, TABLES, & EQUATIONS

Figures

Tables

Equations

INTRODUCTION

Over the last several years, the Boulder Creek Critical Zone Observatory (BcCZO)[1] has been conducting a multitude of interdisciplinary studies in order to more fully comprehend critical zone morphology. The critical zone refers to the near surface of the earth and extends from the air we breathe all the way down to the upper-most regions of solid bedrock (Figure 1). One of the most crucial components of this system is bedrock weathering, since it is a fundamental control on regolith development (Anderson, R. et al., 2011). By quantifying the strength of bedrock, we can better interpret the influence of bedrock weathering on landscape evolution and the critical zone itself.

Within the BcCZO's field area, the Boulder Creek watershed (Colorado), there are three primary research locations: Green Lakes Valley, Gordon Gulch, and Betasso Gulch. Each is unique due to differences such as elevation, climate, and erosional history; therefore, by studying all three, multidimensional interpretations of how the critical zone has evolved and functions can be further developed.

[1] For more on the "feed-through reactor," see (Anderson & von Blanckenburg, 2007).

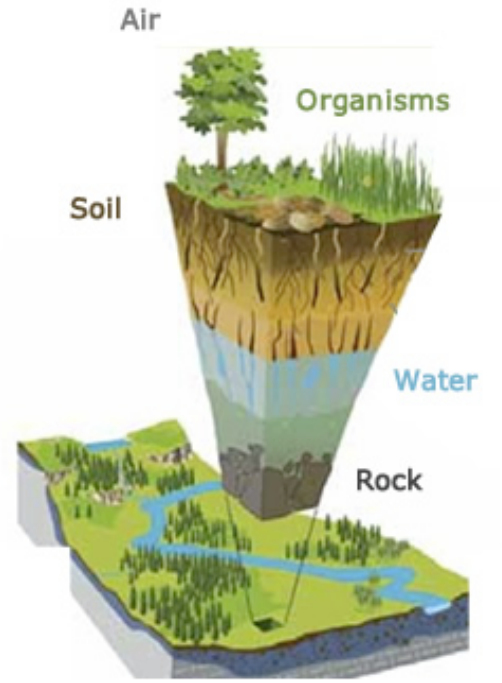

Figure 1: The Critical Zone: an area that extends from the underlying bedrock through to the air above, including weathered rock at all stages of decomposition, water, soil, and vegetation (image from http://criticalzone.org/Research.html).

This study assessed bedrock weathering throughout each of these areas, as well as along three highway road cuts in order to characterize rock strength across an east-west transect of the Boulder Creek watershed. Gordon Gulch in particular has been at the center of many studies investigating hillslope morphology and focusing on observed differences between the north- and south-facing hillslopes (e.g. slope angle, soil development, vegetation, and exposures of bedrock; Dethier and Lazarus, 2006; Anderson et al., 2007; Trotta, 2010; Anderson, S. et al., 2011). Because roughly 10% of the hillslopes in Gordon Gulch are composed of independent bedrock exposures known as tors, this study investigates the

differences between the north- and south-facing slopes through the lens of rock strength and the physical characteristics of these tors. By quantifying the physical and weathering characteristics of these exposures of bedrock, we may be better able to interpret the differences seen between the north- and south-facing hillslopes, which could ultimately assist in explaining hillslope evolution.

Background

Tors

Tors are exposures of rock that are still attached to underlying bedrock and stand independently, with every face free and bare (Figure 2; Street, 1971). More specifically, "a tor is a residual mass of bedrock produced below the surface level by a phase of profound rock rotting effected by groundwater and guided by joint systems, followed by a phase of mechanical stripping of the incoherent products of chemical action," (Linton, 1955).

Topography is one primary influence on where tors develop. For example, in a ridge top setting, there is insufficient groundwater to drive weathering; thus, less rock will rot and there is a higher potential for tor development. However, in locations where there is greater interaction with water, an increased amount of weathering processes can act on the rock, resulting in fewer or more widely spaced tors (Linton, 1955).

Figure 2: An example of a tor in Gordon Gulch (Image from: W. Ouimet).

In this scenario, tor development is strongly related to the structural character of the original, unweathered bedrock. If surfacial erosion is seen as a type of "feed-through reactor," then as "solid material is fed into the reactor through its bottom boundary," erosion can remove solid sediment off the top of the reactor, while the dissolved byproducts of chemical weathering can seep out laterally (Anderson et al., 2007). However, the extent to which weathering can decompose the solid bedrock that is being fed into the bottom of the system is

dependent on the structural characteristics of the rock itself, the most important of which are fractures (Linton, 1955).

Fractures are composed of two parallel, approximately planar surfaces of rock that meet along a fracture front and demonstrate a relative displacement with respect to one another (Pollard and Aydin, 1988). Because fractures create a substantial amount of surface area on which weathering processes can occur, they are not only one of the largest controls on the rate of rock recession and erosion, but also the first step in the process of rock disintegration (Molnar et al., 2007; Moore et al., 2009). For example, with increased fracturing, the rock experiences increased porosity and transmissivity, as well as decreased strength, allowing weathering processes to be more productive (Mabee and Hardcastle, 1997; Ehlen and Wohl, 2002; Molnar et al., 2007). Thus, areas of source rock that have tightly spaced fractures break down and are removed more rapidly than areas with widely spaced fractures (Figure 3). Tors are therefore more likely to form in areas of low density jointing and fracturing, since weathering and erosion will be less productive in these settings.

Tors commonly exhibit differential weathering along their vertical axis. Namely, the tops of tors typically demonstrate more extensive weathering than the bottom flanks. This characteristic can be expressed by the presense of features such as grooves, flutes, gnamas, and pillow structures on the upper parts of tors (Linton, 1955). In Gordon Gulch, it has been determined that the majority of

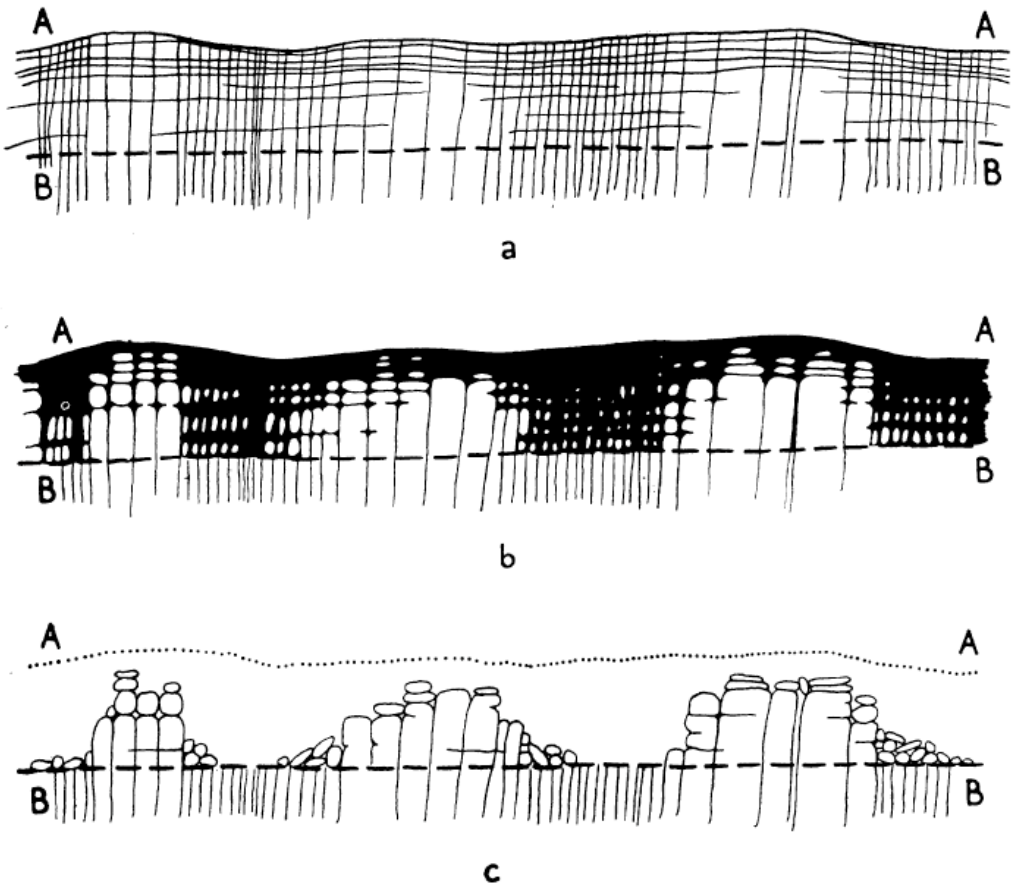

Figure 3: a. Shows the original rock, with variable joint spacing and bedding plane thicknesses illustrated by the black lines. In **b.**, the areas of bedrock that were more jointed have preferentially rotted (black area) and areas with less dense jointing remain more competent. Finally, in **c.**, surficial erosion has removed the rotten rock from **b.**, leaving the more competent rock standing as tors on the landscape. (Lines AA and BB delineate initial and final ground level, respectively). (Image from Linton, 1955)

differential weathering on tors is not attributable to chemical weathering, but rather to the occurance of fractures and physical weathering (Trotta, 2010).

Other research has found that recession and erosion rate can be influenced by uniaxial compressive strength, the orientation of fractures, and topoclimatic situation (i.e. given differential elevation, aspect, inclination, temperature, and precipitation; Moore et al., 2009).

The Schmidt Hammer

The Schmidt Hammer is portable, non-destructive device that measures the unconfined, uniaxial compressive strength of consolidated material (Figure 4). It was first developed by E. Schmidt in 1948 to estimate the strength of concrete installed in buildings and other structures. Several years later, in the early to mid-nineteen sixties, the device was employed to evaluate in-situ disparities in rock strength and coal hardness within mines, which led to its use in the field of civil engineering (Hucka, 1965; Deere and Miller, 1966). Then, in 1977, Day and Goudie published a pivotal study within the field of Geology on the application of the Schmidt Hammer to assess rock strength in the field, claiming that "because elastic recovery [measured by the device]… depends on the hardness of the surface, and hardness is related to mechanical strength, the distance of rebound gives a relative measure of surface hardness or strength," (Day and Goudie, 1977). Since then, geologists have used this device to quickly gauge uniaxial compressive strength in the field.

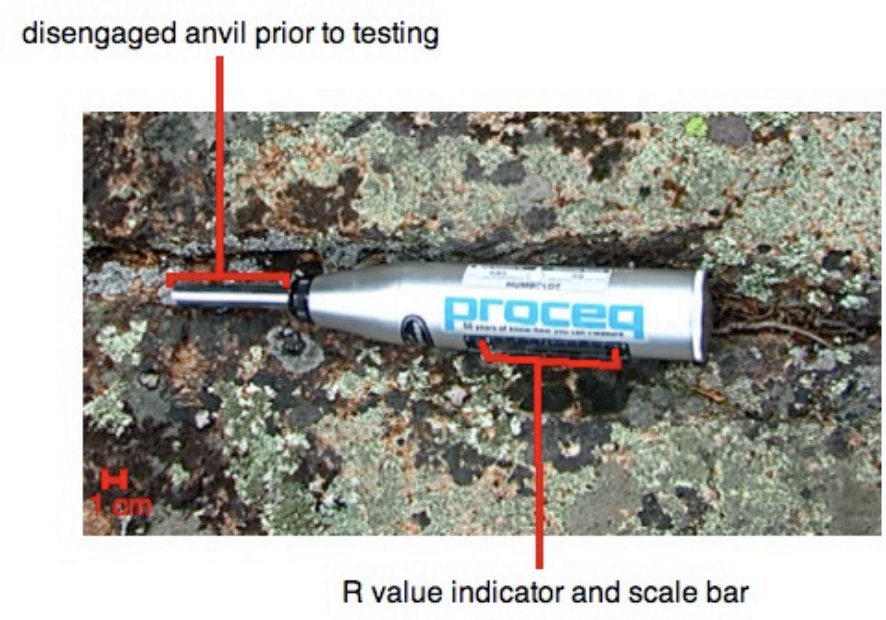

Figure 4: The Schmidt Hammer.

Mechanical Properties and Operator Guidelines

In the most basic sense, the Schmidt Hammer's operation relies on the interaction between its 3 main components: the anvil, piston, and spring (Figure 5). To use the Hammer, the operator positions it perpendicular to the test surface[2] and pushes towards the surface until the anvil is fully engaged within the hammer (Proceq, 2006). When this happens, the piston is loaded by the spring, and then discharges against the anvil, which maintains contact with the test surface (Li et

[2] If the device is not as close to perpendicular as possible to the test surface (deviation should not exceed ± 5°), then "there is a danger of frictional sliding of the plunger tip, material removal by chipping and a partial transfer of energy to and from the hammer," (Aydin and Basu, 2009).

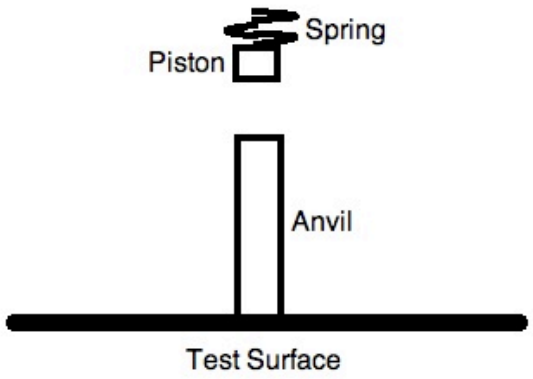

Figure 5: A simplified diagram showing the relationship between the piston, anvil, and spring in the Schmidt Hammer (after Li et al., 2000).

al., 2000). The energy that is released by the impact[3] is mainly either absorbed by plastic deformation of the test surface or transformed into heat and sound. All other energy released facilitates the rebound of the piston, and thus expresses the "impact penetration resistance," or "hardness" of the rock surface being tested (Aydin and Basu, 2005).

When the piston rebounds, the height to which it travels is quantified as a "Rebound" value (R_{value}), which can be read off the side of the device. Weak rock is associated with longer time for the energy wave to penetrate the surface and the wave reaching a deeper extent in the material. This means there is a greater loss

[3] On impact, the *Original Schmidt Hammer Type N*, which was the specific device used for this study, generates approximately 2.207 Newton-meters of kinetic energy.

of kinetic energy from the system and that less energy is reflected back to the piston, causing the piston not to rebound as high in chamber. A smaller rebound in the chamber yields a smaller resultant R_{value}. The same relationship is true of stronger rock, in that a Schmidt Hammer test performed on a stronger surface will yield a larger R_{value} (Aydin and Basu, 2005).

The Schmidt Hammer in Geologic Research

The light, portable nature of the Schmidt Hammer has made it an easy tool to use in the field. Furthermore, because the device yields a specific numerical measurement of hardness, it provides field geologists a way by which to quantify rock decomposition instead of relying on whether or not the rock makes "dull" or "ringing" sounds when it is struck by a standard rock hammer (Geotechnical Control Office, 1988a). "However, a number of issues such as hammer type, normalization of rebound values, specimen dimensions, surface smoothness, weathering and moisture content," as well as "testing, data reduction and analysis procedures continue to undermine the reliability of the Schmidt Hammer," (Aydin and Basu, 2005)[4].

In the defense of the Schmidt Hammer, it is used to measure intact rock strength, which is the material strength between discontinuities. When testing compressive strength in the lab, drilled cores are used, which are intrinsically

[4] For more research on issues that cloud unanimous approval of the Schmidt Hammer: (Li et. al., 2000; Aydin and Basu, 2005; Goudie, 2006; Niedzielsk et. al., 2009; Aydin, 2009; Viles et. al., 2011)

representative of the best of the drilled sample and not necessarily representative of the entire body of rock. On the other hand, if there are many discontinuities within the core, the lab test will only really be assessing the strength of those discontinuities. Furthermore, if there is evidence of anisotropy within the sample, then orientation can become an important factor. Thus, laboratory testing is not without limitations. While the Schmidt Hammer can also be influenced by discontinuities (since there is no way of knowing what discontinuities are within its sphere of influence) it has been shown that a "characteristic mean strength value of a unit is better determined by a large quantity of estimated values than by a few," tests of unconfined compressive strength (Hack and Huisman, 2002).

Factors that Influence Schmidt Hammer Rebound (R_{value})

There are several ways in which the Schmidt Hammer can overestimate and underestimate rock strength. One of the most common affecting factors is the angle (with respect to normal) at which the device is used. If the device is used between +1° to +90°, the force of gravity will act to dampen the piston's rebound, and thus reduce the R_{value}. On the other hand, if the device is used at an angle below the normal (-1° to -90°), then the force of gravity will exaggerate rebound, and thus increase the R_{value}. As shown in Figure 6, the incidence angle can cause an over- or under-estimate in R_{value} between 7 to 73% (the effect of incidence angle is the greatest when testing rock of lower compressive strength, up to 73%

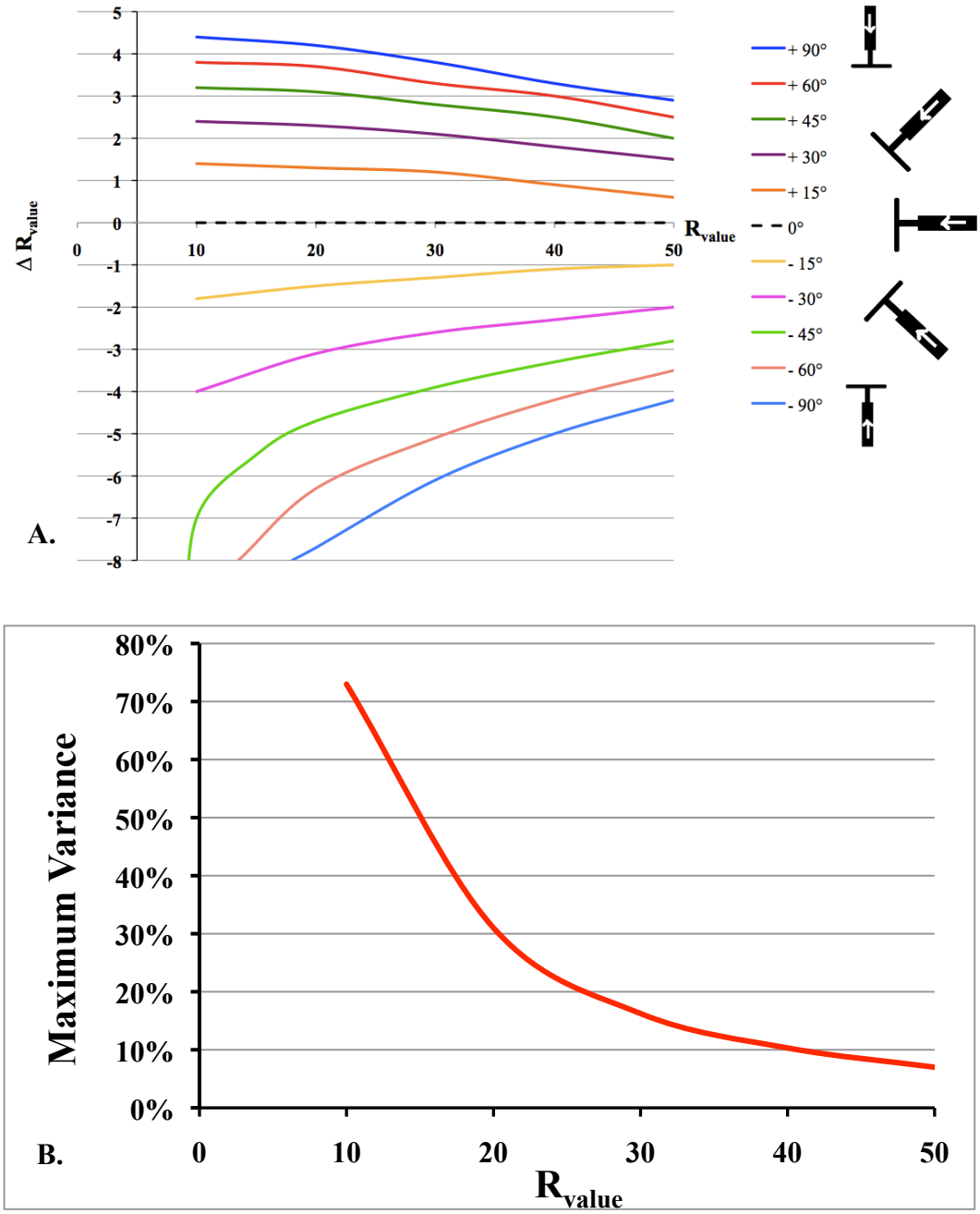

Figure 6: A. Influence of incidence angle on measured R_{value}, a given ΔR_{value} should be added to the measured R_{value} to correct for the influence of gravity (adapted from ELE International, Inc., RM-710 technical data). **B.** The maximum percent variance in R_{value} for each rebound measurement caused by incidence angle (adapted from **A**).

variability, and lowest when testing stronger rock, closer to only 7% potential variance). This means that R_{values} that are not corrected for incidence angle will demonstrate a broader range of Schmidt Hammer rebound measurements.

There are also other influencing factors on the Schmidt Hammer that can complicate measurements. For example, an underestimate could result from an unbuffed or unprepared test surface, since some of the kinetic energy in the system will be lost to pieces of rock that have broken off of the test surface due to the Hammer's impact. Likewise, R_{values} could be diminished if measurements were taken near a subsurface fracture in the rock, which would absorb energy from the system. Therefore, multiple factors must be accounted for when considering what the R_{value} produced by a Schmidt Hammer actually represents.

Previous Work

Gordon Gulch

In 2010, Trotta conducted extensive research on the distribution of tors in Gordon Gulch. Based on thorough mapping and the use of geospatial analysis programs, he determined that gneissic tors make up the most tor area, but are not as tall as granitic tors (Trotta, 2010). The aspect of tors in Gordon Gulch was found to be roughly 66% south-facing, and only about 1/3 as many tors with

north-facing aspect. Overall, the south-facing slopes were found to have the largest and most dense tors in the gulch (Trotta, 2010).

The majority of the tors are located in some of the steepest areas of the gulch, although not all of the steepest areas have tors and not all areas of low slope are free of tors (Trotta, 2010). In his study, Trotta relied on mathematical conceptions of mass movement to explain the prevelance of tors on the steep south-facing slopes. He argued that since the erosive processes that expose tors are mainly determined by shear stress, which is derived from slope angle and soil moisture, an increase in erosion could be correlated to an increase in slope angle and soil moisture, resulting in more tors (Trotta, 2010).

Alternatively, Trotta proposed that since "it has been shown that climate differences between two slopes (primarily driven by differences in solar insulation) are strong enough to have a significant effect on plant life," perhaps the aspect driven microclimates in Gordon Gulch, and the resultant differences in vegetation cover, dictate the variation in erosion (Trotta, 2010).

Modeling the "Feed-Though Reactor"

When the principle of the Critical Zone behaving as a "feed-through reactor" is modeled in an effort to understand hillslope evolution, not only does "rate of detachment of rock into the mobile regolith layer, rate of mobile regolith transport, and channel incision or aggradation rates," need to be considered, but also "the evolution of material within the weathered bedrock," (Anderson, R. et

al., 2011). Anderson's models attempt to account for these factors in a process-oriented fashion that models how each part of the progression occurs, instead of measuring end results, such as soil thickness. One of his model's key factors is "damage," (which is how he characterizes weathering), which damage directly results "in [a] reduction of physical strength [of the rock, and its] ability to resist deformation under stress," (Anderson, R. et al., 2011). Data collected with a Schmidt Hammer, such as the data collected for this study, could provide viable numeric values that quantify what Anderson refers to as "damage," ultimately enhancing the scope and accuracy of the model.

GEOLOGIC & CLIMATIC SETTING

Geologic History

This study was conducted in the Colorado Front Range, a mountain belt roughly 180 miles long and 40 miles wide within the Southern Rocky Mountains (Figure 7; Sonnenbery and Bolyard, 1997). The oldest rocks within the Front Range have been dated to the Proterozoic, and have undergone a complex geologic history over the last 1,790 million years. This history is described by Kellogg et al. (2008) as four primary phases of development:

> *Precambrian:* During the Precambrian, this area experienced the initiation of an orogenic period that would stretch from 1,790 Ma until the Mesozoic (~130 Ma), and it was in the early phases of this orogeny that the Proterozoic rocks that compose the core of the Front Range came into existence. Marine sediments, as well as volcanic rocks, experienced ductile deformation, high pressure and low temperature metamorphism, and granitic intrusions. En

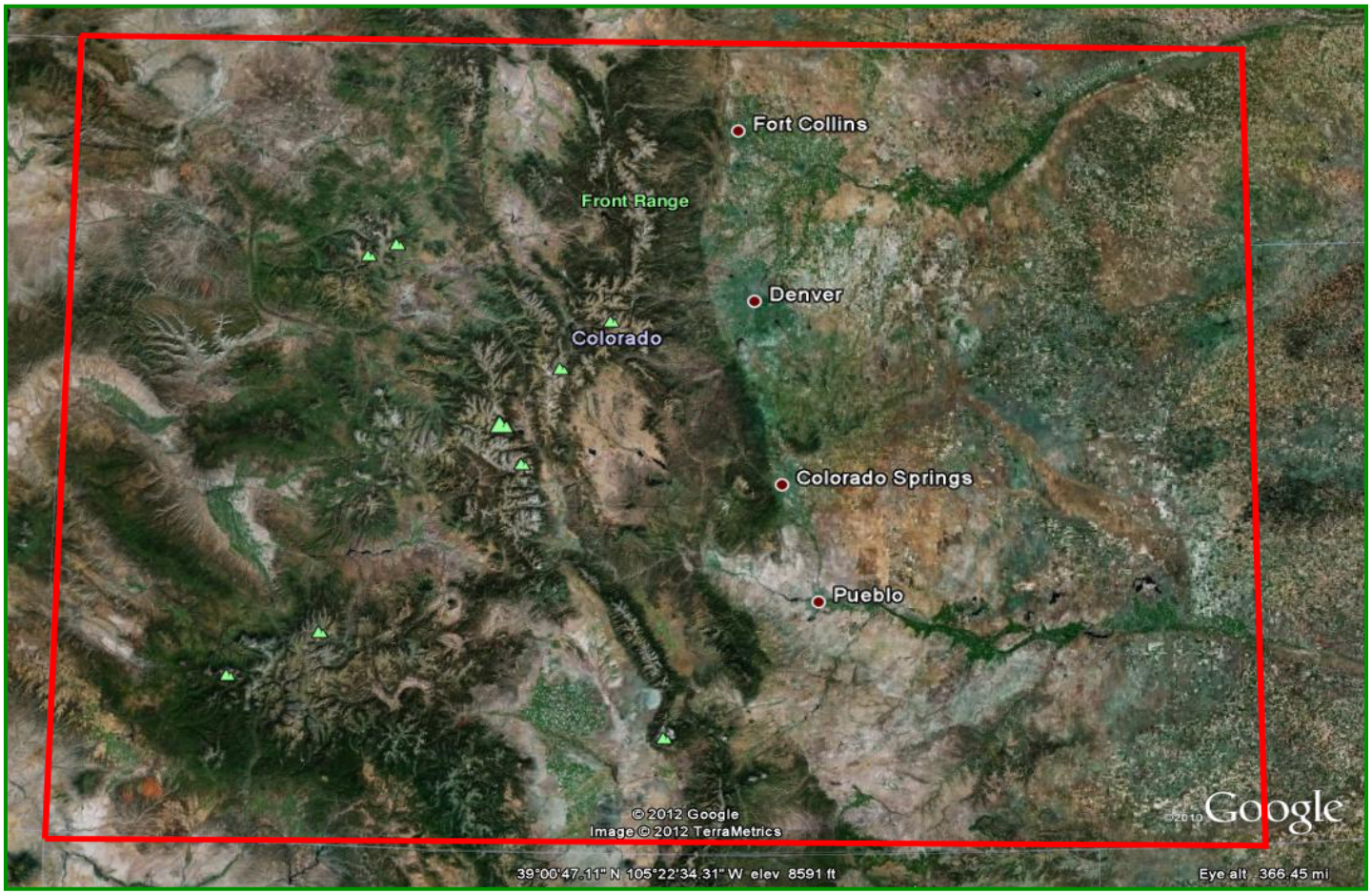

Figure 7: The State of Colorado (outlined in red). The Front Range (where this study took place) is labeled in green (Image from: Google Maps).

echelon shear zones, trending East/Northeast, dominated the tectonic regime and several periods of plutonism formed a multitude of dikes, country rock inclusions, and complex local contacts (Sonnenbery and Bolyard, 1997). For example, one such phase of plutonism, occurring around 1,420 ±25 Ma produced the granite of Longs Peak Batholith (Peterman, 1968), which is one of the lithologies examined in this study.

Paleozoic & Pre-Laramide Mesozoic: In the early Paleozoic, sands and carbonates accumulated on a broad continental shelf; but, by later in the era, the Ancestral Rocky Mountain Orogeny uplifted and eroded these sediments. In the Middle Jurassic, fluvial and lacustrine deposits blanket the Ancestral Front Range, which had been eroded to very low levels of relief, and by the initiation of the Middle Cretaceous, substantial subsidence allowed for the western interior seaway to entirely subsume the Ancestral Rocky Mountains (Kellogg et al., 2008).

Laramide Orogeny: From approximately 80 – 40 Ma, the Laramide Orogeny built the modern Rocky Mountains and Front Range (Dickinson et al., 1988). This period saw not only rapid uplift and intense crustal shortening, but also the recession of the western

interior seaway (post 69 Ma, which deposited such coastal plain sediments as the Laramie Formation - the namesake of the orogeny), as well as the erosion of Paleozoic and Mesozoic sediments in excess of 2 km (Kellogg et al., 2008). However, the loading caused by the Laramide Orogeny is thought to have been "superimposed on long-term regional subsidence," which continued after the orogeny until roughly 8 – 6 Ma, and carried on in the peripheral regions until 4 – 3 Ma (McMillan et al., 2006).

Post-Laramide: After the Laramide Orogeny, the region continuously fluctuated between periods of intensified erosion and smaller uplift events throughout much of the Cenozoic. Variations in fluvial erosion rates were closely related to climatic oscillations, but were also amplified by exaggerations in local relief due to uplift (Kellogg et al., 2008). In the Quaternary, there have been at least 12 distinct glaciations in the Front Range. It is assumed that most glaciations before Marine Oxygen Isotope Stage 16 were probably less extensive in the Front Range than both the Bull Lake (pentultimate) and the Pinedale (most recent major) glaciations. Both of these most recent events are associated with local glaciers as long as 10 – 20 km, with thicknesses ranging from 180 – 350 m. They are believed to have extended down to elevations as low as

2,500 – 2,700 m (roughly to where the modern Peak-to-Peak Highway is located) and deposits from the Pinedale have been dated to roughly 30-12 Ka (Kellogg et al., 2008).

Climate: The current climate in the Front Range area varies from West to East as the elevation decreases from around 4,000 m in the alpine to 1,600 m in the Boulder area. In the high alpine regions, precipitation exceeds a mean of 100 cm annually, with mean runoff measured as 150 cm. In Boulder, mean annual precipitation hovers near 46 cm and runoff at 10 cm. Mean annual temperature is also vastly different along this West to East gradient, ranging from – 4° C in the mountains to 11° C in Boulder. As a result of the change in temperature and precipitation, we see a large change in vegetation as well. The Boulder area can be characterized as predominently a grassland regime, with the amount of vegetation and percentage of evergreen forest cover increasing with the topography until roughly 3,450 m, when tundra dominates the landscape (Dethier and Lazarus, 2006).

Primary Rock Types Observed

The primary rock types examined in this study include: Paleoproterozoic biotite schists and gneisses, Boulder Creek granodiorite, and the granite of Long's Peak batholith. To facilitate a broad and inclusive comparison of rock strength across lithologies, two primary lithologic groups were identified in the field, the "metasedimentary" suite (the Paleoproterozoic biotite schists and gneisses) and a "granitic" assemblage (the Boulder Creek granodiorite and granite of Long's Peak batholith).

Paleoproterozoic Biotite Schist and Gneiss

(*found in Gordon Gulch, Green Lakes Basin, and the highway road cuts*) High grade metamorphism formed these metasedimentary rocks around 1,713 ±30 Ma (Cole and Braddock, 2009). Due to metamorphic segregation, the affects of partial melting, and inherited differences from the original sedimentary sequence, this rock is complexly and irregularly banded, and locally can include bands of quartzofeldspathic and knotted mica schists (Kellogg et al., 2008). The rock is well foliated and has darker shades of grey and black interbedded with lighter greys. Grain size can be observed in different localities to be characteristically fine, medium, or coarse. Primary minerals are biotite, sillimanite, magnetite, high-grade cordierite or garnet (Cole and Braddock, 2009). More specific studies have shown the composition to be "approximately 25–50 percent quartz, 20–30 percent plagioclase (approximately An_{30}), 0–30 percent microcline, 10–15 percent

biotite, 0–15 percent muscovite, 0–10 percent sillimanite, 0–5 percent hornblende, 1–2 percent opaque minerals, and a trace zircon," (Kellogg et al., 2008).

Boulder Creek Granodiorite

(*found in Gordon Gulch and Betasso*) This granodiorite is a Paleoproterozic intrusive rock that has been dated to 1,716 ±3 Ma (Kellogg et al., 2008). It is medium to light grey in color and medium to coarse grained. There are many pegmatitic veins present through the rock (especially in Betasso) and it varies between being equigranular and porphyritic, as well as massive to weakly foliated. Primary constituents are quartz and feldspar, with "5–15 percent biotite and 0–5 percent hornblende," (Cole and Braddock, 2009).

Granite of Longs Peak Batholith

(*found in Gordon Gulch, Green Lakes Basin, and the highway road cuts*) In the field, this rock was referred to as "Silver Plume Granite;" however, further research has shown that it is more aptly classified as granite of Longs Peak Batholith.[5] The rock is a light grey to grey, equigranular granite that varies between having fine, medium or coarse grains. "Biotite is the principal dark mineral (5–12 percent), locally accompanied by magmatic sillimanite and (or) garnet plus minor accessory minerals," (Cole and Braddock, 2009).

[5] It is a prevailing habit of Front Range geologists to label many types of granite that are similar in age and display very similar compositional and textural characteristics as the same rock. However, while the rocks may be very similar, typically they are from separate batholiths, and thus should be identified separately (Kellogg et al., 2008).

Field Locations

Four locations were selected for this project: Gordon Gulch, Betasso Gulch (road cuts along Betasso Road and Bummer's Rock), Green Lakes Basin, and three highway road cuts (Figure 8). Other than the road cuts, these areas make up the primary research locations for the Boulder Creek Critical Zone Observatory (BcCZO). Each location is valued for its distinct geologic and climatic history, which intrinsically provides the basis for comparative analysis.

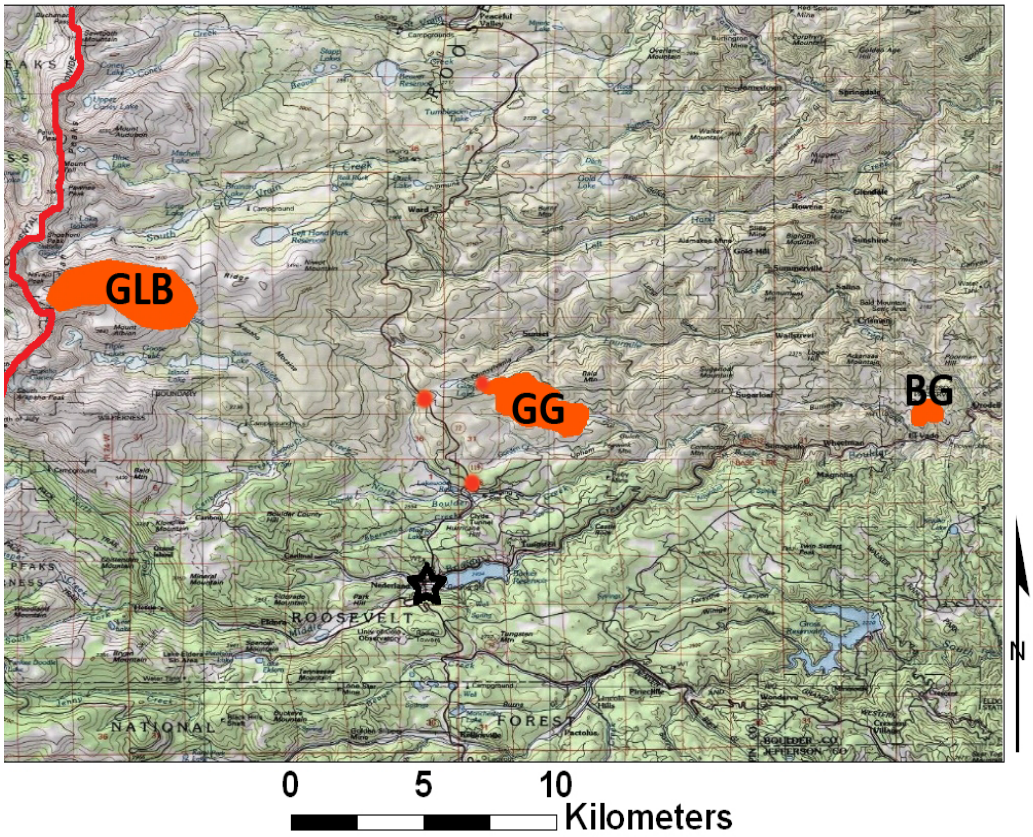

Figure 8: Map of field locations GLB=Green Lakes Basin, GG=Gordon Gulch, and BG=Betasso Gulch. The small orange points are the road cuts. A black star marks the town of Nederland and the red line indicates the Continental Divide.

Green Lakes Basin

Green Lakes Basin, situated above 3,300 m elevation, is the high elevation end member out of all of the locations (Figure 9). The basin was repeatedly glaciated and deglaciated throughout the Quaternary, with the last major deglaciation occurring roughly 15 Ka. The Arapahoe Glacier is located at the top of the basin and feeds a series of six pro-glacial lakes. The lower four lakes have been dammed, while the upper two are separated from them by a roughly 100 m bedrock step. The vegetation in this area is predominately indicative of an alpine tundra landscape, although there is evergreen forest at its lowest reaches. The test sites chosen in Green Lakes Basin are predominantly glacially polished bedrock and adjacent outcrops of weathered bedrock.

Gordon Gulch

Gordon Gulch is a small catchment within the Boulder Creek Watershed that, at elevations between roughly 2,400 – 2,700 m, provides a middle elevation for this project (Figure 2). Unlike Green Lakes Basin, this area is outside of the glacial limits and sustains a much broader array of vegetation. That being said, there is a significant disparity from one side of the valley to the other in a variety of characteristics, such as ecology and density of vegetation. The specific test sites chosen in Gordon Gulch were meant to represent variations in lithology, slope orientation, and relative location within the gulch as well as on the tor itself. Soil pits were also tested if they were deep enough to expose bedrock (typical pit

depths were between 0.75 – 1.25 m). These were mostly abandoned mine-prospecting pits, but several were pits dug for concurrent field studies.

Figure 9: Green Lakes Basin, looking up-valley at Lake 4 from Niwot Ridge.

Road Cuts

Of the three highway road cuts (Figures 10-12) studied for this project, two were along the Peak-to-Peak highway ("AR1" and "AR2") and the third was on the abandoned "Switzerland Trail," a 19th century railroad ("AR3"). Each location represents a primary local lithology (granitic, gneissic, and schistose,

respectfully), but also the freshest rock in the area, since it was exposed within the last half century.

Figure 10: AR1: granitic road cut, as seen from the Peak-to-Peak Highway, resembles a tor-like structure, rather than continuous bedrock (Image from: D. Dethier).

Figure 11: AR2: gneissic road cut, as seen from the Peak-to-Peak Highway (Image from: D. Dethier).

Figure 12: AR3: schistose road cut, as seen from the Old Switzerland Railroad (Image from: D. Dethier).

Betasso Gulch

The Betasso Gulch field area is representative of the lowest elevations considered in this study (Figure 13). Locations tested within this area were at elevations of roughly 2,000 m (±20 m), and show a local contrast at that elevation between grus and saprolite compared to more competent tors (e.g. Bummer's Rock). This is the low elevation end member of this group of field areas.

Figure 13: The Betasso Gulch field area, along Betasso Road (Image from: D. Dethier).

Figure 14: Bummer's Rock, a ridge top tor in Betasso Gulch. View to the north-east. In the distance, Betasso Road enters from the left and ends at the Betasso Water Treatment Plant on the right (Image from: D. Dethier).

METHODS

Both field and laboratory methods were used to quantify rock strength and to assess its influence on hillslope development. The primary characteristics that have been taken into consideration for this project include: uniaxial compressive strength (as measured in the field and in the laboratory), fracture spacing, fracture orientation, rock type, and location /climatic setting. Measurements of uniaxial compressive strength from the Schmidt Hammer as well as fracture orientation and spacing were collected in the field along with descriptions of rock type and location. Further assessment of uniaxial compressive strength in the laboratory and evaluations of the impact of location /climatic setting were done via spatial and graphical analysis. Outlined below are the methods implemented both in the field and in the laboratory.

Field Methods

Locations

For every site visited in the field, a GPS coordinate was taken with a Garmin *E-Trex* to mark its location in space. Uncertainty values were deemed acceptable if they were reported as 6 meters or less by the device. Furthermore, the rock at each locality was identified and a brief description of the surface tested with the Schmidt Hammer was recorded.

Schmidt Hammer Measurements

Schmidt Hammer measurements were taken at every location examined for this study to obtain a non-destructive measurement of uniaxial compressive strength in the field (see *Introduction:* Background).

Based on Linton's observations of vertical weathering differences on tors, the top of the tor should, in theory, be more weathered than the base (1955). To test Linton's theory, as well as to investigate whether or not this difference in weathering could be quantified by variations in compressive strength, the Schmidt Hammer was used to test faces of differing orientation on each tor. Three types of tor faces were identified and measured: top, up-slope, and down-slope (Figure 15).

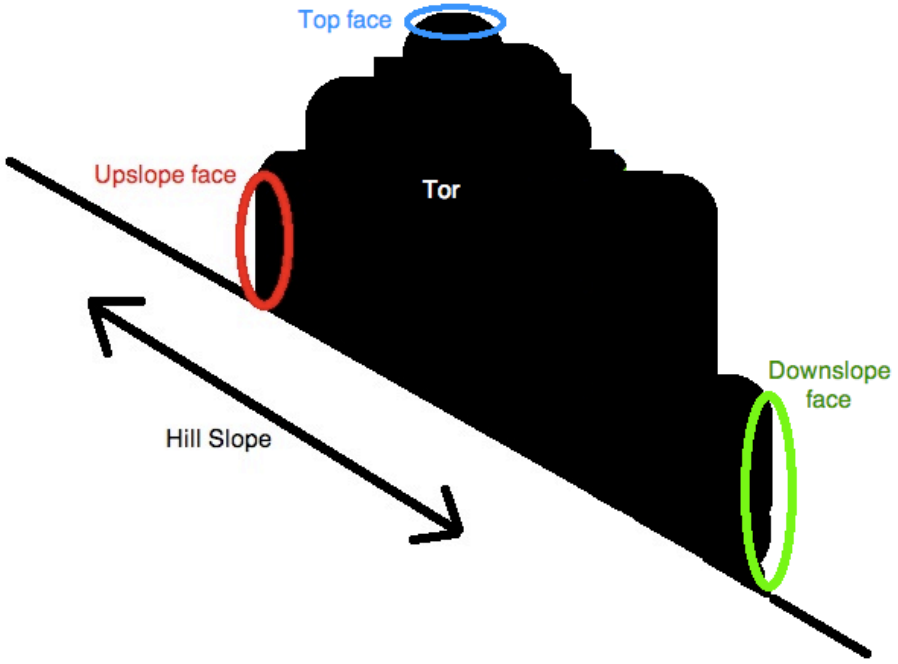

Figure 15: Illustrates the relative locations of "up slope," "down slope," and "top" faces on a tor.

The faces chosen for testing were the smoothest (less than 5mm amplitude of surface texture) and least lichen-covered areas. The Schmidt Hammer was carefully positioned perpendicular to the rock surface in adherence with the manufacturer's operator instructions (Proceq, 2006). However, since many of the guidelines dictated by the manufacturer, and used in most tests involving the Schmidt Hammer, were unknown while in the field, they were not strictly followed. This includes buffing/preparing the test surface and recording the angle of the Hammer from horizontal (incidence angle) while testing. The resulting measurements were then recorded either by the operator or a field assistant

(Figure 16). Early on in the testing period, twenty measurements were taken at different discrete points in a $1m^2$ area. The number of measurements taken was later modified to thirty discrete measurements on a $1m^2$ rock face, with an additional ten measurements taken if the initial yield seemed inconsistent.[6]

Figure 16: The author operating the Schmidt Hammer in the Green Lakes Basin field area (Image from: D. Dethier).

[6] This change was implemented for the purpose of improving the statistical analysis of the data. The assumption was that the higher the sample number, the less impact faulty outliers would have on statistical computations. The majority of test sites were measured 30 different times.

In the case of the Green Lakes Basin field area, the tested locations were not tors, but rather glacially polished and exposed bedrock surfaces. These surfaces were chosen because they were assumed to be the least weathered surfaces in the area. That being said, Schmidt Hammer measurements were taken on several weathered surfaces immediately adjacent to the polished surfaces for comparative purposes. At each of these locations, the same methods of data collection were followed.

At highway road cuts, prospecting pits, and pits recently dug for soil analysis, sampling was conducted systematically from top to bottom. If the rock face was less than 5m high, then measurements were taken close to the middle of the surface in the smoothest area. If, however, the rock face was in excess of 5m in height, then measurements were taken at the approximate bottom, middle and top of the rock face. In these cases, the relative height of the road cut and the height of the measurement location were measured with a laser rangefinder. Lastly, if the Schmidt Hammer measurements were taken in a pit with exposed bedrock exceeding $1m^2$ in area, then multiple test locations were used and the depths reported with respect to the surface of the soil with a measuring tape.

Fracture Spacing

Fracture spacing was measured at every tor within Gordon Gulch to determine whether or not there is a link between large-scale fracture density, the Schmidt Hammer's measurement of uniaxial compressive strength, and

topographic relief. The faces chosen were deemed representative of the overall fracture pattern present at each tor. On several occasions there were multiple faces of the tor that represented prevalent fracture patterns, for these tors there are multiple sets of fracture spacing measurements.

Once a representative face was selected, a measuring tape was held perpendicular to fractures along the face of the tor (often by multiple field assistants) and parallel to the ground. The tape was positioned so that the 0cm marker was on a fracture. A recorder then walked down the length of the tape, noting the number of centimeters from the original fracture where each subsequent fracture intersected the measuring tape transect. This continued until the recorder reached the last fracture apparent on the face. Fractures were deemed noteworthy in this process if they were at least 1m in length, and if a fracture did not physically intersect the measuring tape transect due to the removal of rock from the tor, the line of the fracture was projected down to the transect (Figure 17).

Fracture spacing measurements were also taken at Betasso and followed the same methodology outlined above. The one exception being that the locations sampled in Betasso were road cuts not tors; therefore, only one face was measureable.

Figure 17: The solid red line represents the measuring tape that was held parallel to the ground and straight along the tor. The smaller dashed red lines indicate fractures where a measurement would have been taken. The measuring transect would both begin and end at a fracture plane.

Fracture Orientation

At each tor examined in Gordon Gulch, the orientation of the fracture planes were measured with a Brunton compass to ascertain if the orientation of the fractures are impacting local variations in topographic relief. For tors composed of metasediment showing distinct foliation planes, the orientation of

foliation was measured with a Brunton compass as well to evaluate if the orientation of the foliation was affecting the hill slopes in Gordon Gulch.[7]

Sampling

Rock samples of each rock type from each field area were collected in the field for subsequent evaluation in the laboratory. Generally, the hand samples were between 5 and 10 cm.

Laboratory Methods

Uniaxial Compressive Strength (UCS) Test

To further evaluate rock strength the samples collected in the field were tested in the laboratory to assess their uniaxial compressive strength. The compressive strength of the samples measured in the laboratory test were then compared to the measurements of uniaxial compressive strength taken in the field with the Schmidt Hammer, providing a way in which to determine the accuracy of the measurements taken in the field.

Samples were cored using a drill press, and were only viable for testing if they were at least twice as long in length as in diameter (so that the failure

[7] Neither fracture orientation, nor foliation orientation, were measured at any of the other field locations, since the purpose of studying those other areas was to provide contrast and comparison for the Schmidt Hammer measurements taken in Gordon Gulch, and not to quantify the factors impacting the local hill slopes.

fracture was entirely contained within the sample – if the failure planes do not terminate within the height of the sample, but rather extend through the end of the sample, the resulting measurement is most likely over-exaggerated). Due to the fact that most samples collected were very small (most only 7 – 10 cm across), they were drilled with a 1-inch diameter coring drill to produce cores that were 2.5 cm in diameter and 5.1 cm in height. Once samples were drilled, they were trimmed with a rotary saw and buffed to produce ends that were parallel to one another.

To test the uniaxial compressive strength of the samples, they were each oriented vertically in an ELE uniaxial compression testing machine (Figure 18). They were placed on top of a steel platform (because the machine was designed to test much larger cylinders of concrete) and between two caps filled with a rubber-like substance to correct for any slight discrepancies that the core may have between bases (i.e. not being perfectly parallel). The initial hydraulic pressure exerted by the machine was recorded before force was exerted on the sample. Then a hydraulic pump continuously exerted increasing amounts of force on the sample, until the sample failed. The maximum hydraulic pressure that was in the chamber at the point of failure was recorded.

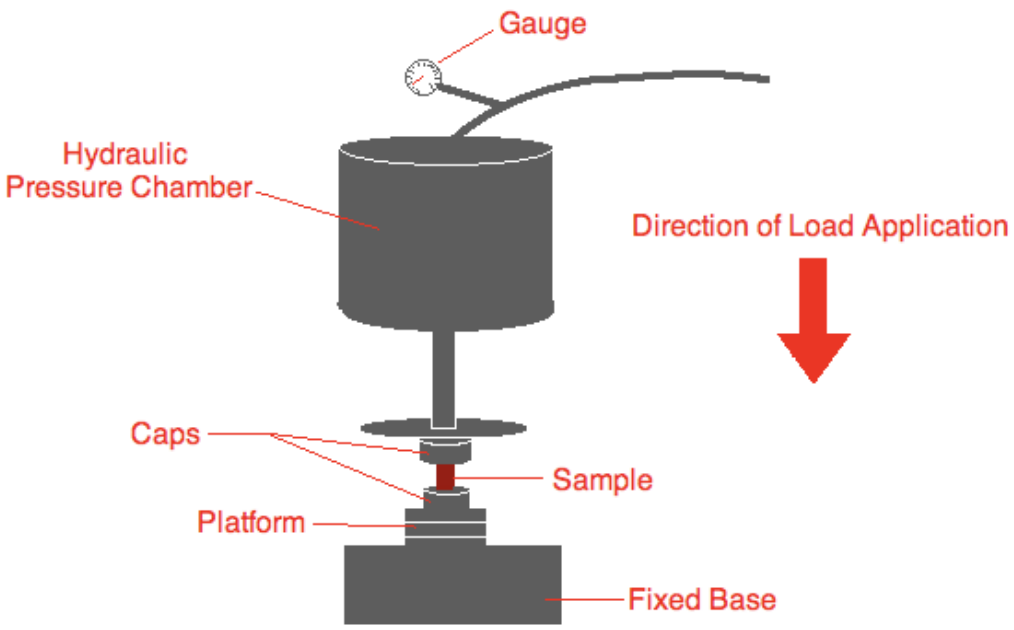

Figure 18: ELE Uniaxial Compressive Strength Test Machine. Sample is capped to account for any slight imperfections on the core bases. Load is applied and Pressure is measured by the attached gauge until sample failure.

To find the effective stress on the sample at the time of failure, the total force being exerted by the device must be calculated:

$$F_{Total} = P_{Hydraulic} \bullet A_{Actuator} \qquad \text{(Eqn. 1)}$$

Where F_{Total} is the total force applied (N), $P_{Hydraulic}$ is the hydraulic pressure (recorded from gauge, psi), and $A_{Actuator}$ is the area of the actuator (m^2). Then, to determine the stress on the sample:

$$\text{Stress on Sample} = \frac{F_{Total}}{A_{Sample}} \qquad \text{(Eqn. 2)}$$

Where Stress on Sample (Pa), F_{Total} is calculated from Eqn.1 (N), and A_{Sample} is the area of the sample (m^2). Unit conversions were necessary, and ultimately results were reported in Mega-Pascals.

Analytical Methods

Analysis of Schmidt Hammer Data

To analyze Schmidt Hammer data, the way in which the Hammer operates must be taken into account. As mentioned previously, there are multiple factors that can influence the R_{value} measured by a Schmidt Hammer. These factors illustrate how the Schmidt Hammer can underestimate, and occasionally overestimate, compressive strength, which ultimately means that the Schmidt Hammer does not generate data sets with Gaussian distribution. Therefore, the statistical analysis of Schmidt Hammer data should not be based on measures of variability such as standard deviation, but should instead consider the great likelihood of underestimation and the marginal chance of overestimation. Thus, the use of quartiles, namely the 3rd quartile, as well as direct analysis of data distribution and mean R_{values} are more helpful for examining the resultant data sets (M. Cooke, University of Massachussets, Amherst, personal communication, Feb, 2012).

Geospatial Analysis

The geospatial analyses of slope aspect and krig-ing were processed using ArcMap, version 10.

RESULTS

Rock Strength Measurements

Analysis of the Schmidt Hammer with Respect to Uniaxial Compressive Strength

Laboratory testing of uniaxial compressive strength (UCS) was completed with 3 cores, all from fresh/unweathered road cuts, to assess the consistency of the relationship between Schmidt Hammer rebound (SHR) and UCS. Two of the samples tested were classified as granitic (a quartz-monzonite and a granite) and the third as metasedimentary (gneiss). The granitic rocks failed under 111.7 MPa and 110.2 MPa of uniaxial compressive stress; whereas, the gneiss failed under 184.7 MPa of uniaxial compressive stress (Table 1). These UCS measurements were then compared with the SHR measurements to assess the correlation between values (Figure 19). Published correlations between UCS and SHR are typically defined as a logarithmic relationship (Deere and Miller, 1966); however, the data collected in this study do not plot on this curve, but rather fall below the curve, indicating that either the Schmidt Hammer over-estimated, or the laboratory tests under-estimated, rock strength. Therefore, the measured

quantifications of SHR shall be assessed comparatively with one another, and not in terms of UCS.

Table 1: Hydraulic pressure (psi) recorded at sample failure, as well as the corresponding pressure converted to MPa and proportioned for stress/area for the three rock samples tested in the laboratory.

Rock Sample	psi reading at failure	stress on sample (MPa)
AR1 (Quartz-Monzonite)	200	111.7
GL17 (Granite)	197	110.2
GL17 (Gneiss)	350	184.7

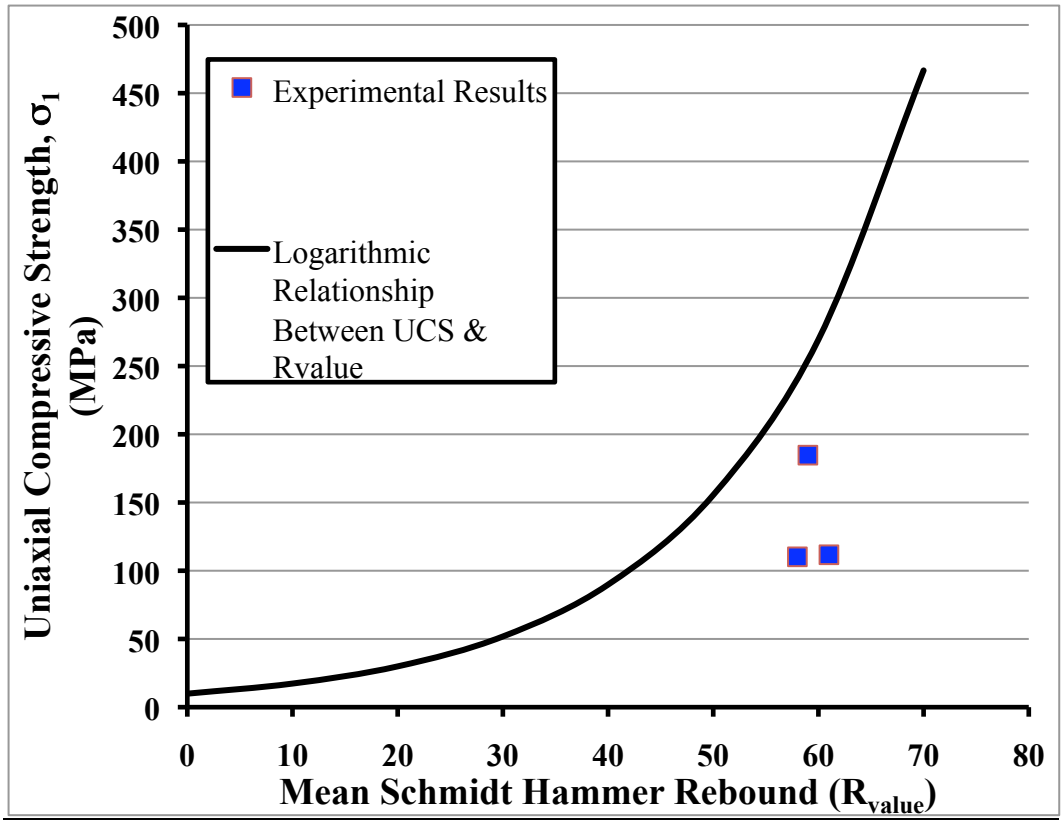

Figure 19: The logarithmic relationship between UCS and SHR taken from Deere and Miller (1966) is compared to the experimental correlation data, showing that the particular Schmidt Hammer used in this study appears to overestimate UCS.

Variations in Rock Strength Due to Lithology

To test if different lithologies can be distinguished based on a quantification of their uniaxial compressive strength (UCS), the UCS of unweathered metasedimentary (Paleo-Proterozoic biotite schist and gneiss) and unweathered granitic (granite of Long's Peak Batholith and Boulder Creek granodiorite) bedrock was measured with the Schmidt Hammer (Figure 20A). The Schmidt Hammer rebound (SHR) for the unweathered metasedimentary bedrock varied from 39 to 66 R_{value}, had a 3rd quartile range between 57 and 60

R_{value}, and a mean SHR of 55 R_{value} (n=16). The unweathered granitic bedrock varied from 39 to 69 R_{value} and had a 3rd quartile range between 60 and 61 R_{value}, and a mean SHR of 55 R_{value} (n=9), identical to the unweathered metasedimentary rocks tested.

Weathered bedrock of both lithologic groups was also examined across the landscape and yielded similar results (Figure 20B). The Schmidt Hammer rebound (SHR) for the weathered metasedimentary bedrock varied from 25 to 51 R_{value}, had a 3rd quartile range between 39 and 43 R_{value}, and a mean SHR of 39 R_{value} (n=24). The weathered granitic bedrock varied from 23 to 56 R_{value}, had a 3rd quartile range between 36 and 42 R_{value}, and a mean SHR of 36 R_{value} (n=23) similar to the unweathered metasedimentary rocks tested.

A.

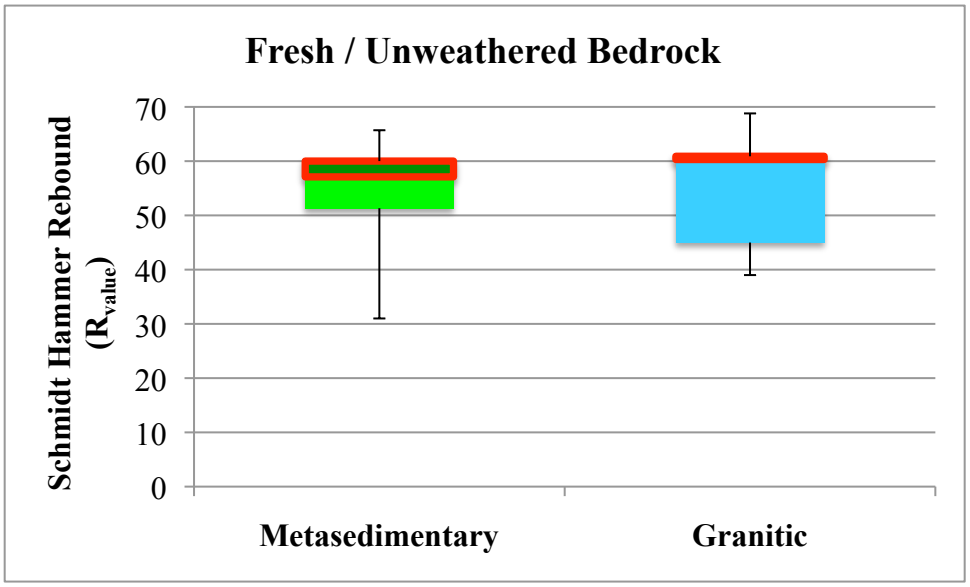

B.

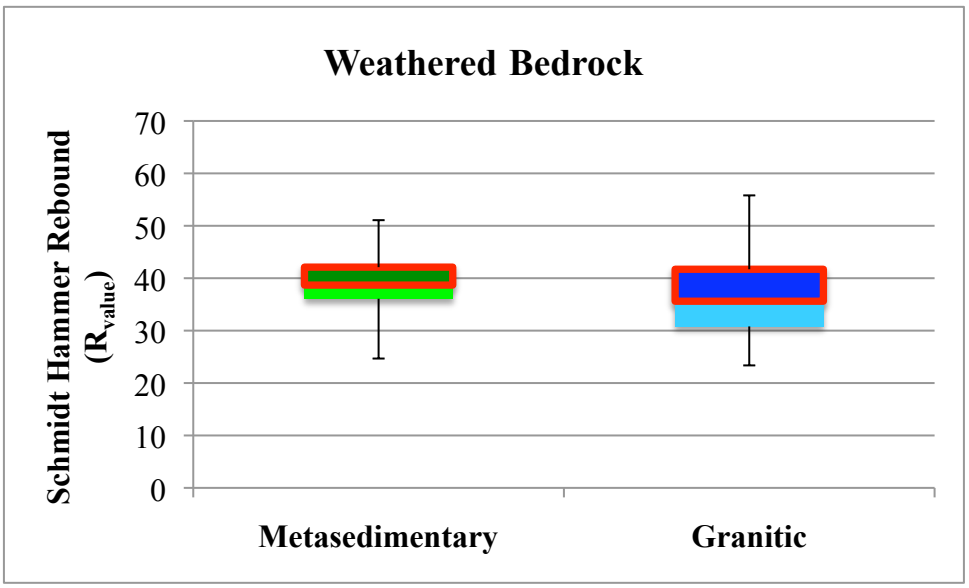

Figure 20: Box/Whisker plot of Schmidt Hammer R_{values} with respect to lithology. Thick red lines circumscribe the 3rd quartiles of each data set. **A.** illustrates that unweathered bedrock throughout the watershed, of both lithologies, is similar in strength. Similarly, **B.** demonstrates that weathered bedrock throughout the watershed, of both lithologies, is similar in strength.

While lithology does not appear to influence the SHR measurements of the rocks sampled in this study, specific characteristics of a lithology, such as foliation, may affect the strength measured. To evaluate the influence of Schmidt Hammer orientation with respect to foliation, the Hammer was used both parallel and perpendicular to foliation on various exposures of metasedimentary bedrock. The 3rd quartile range of the data when the Schmidt Hammer was used parallel to foliation planes was between 41 and 46 R_{value}, and between 40 and 48 R_{value} when used perpendicular to foliation. However, for both orientations of the Schmidt Hammer with respect to foliation, the mean SHR was identical (41 R_{value}; Figure 21).

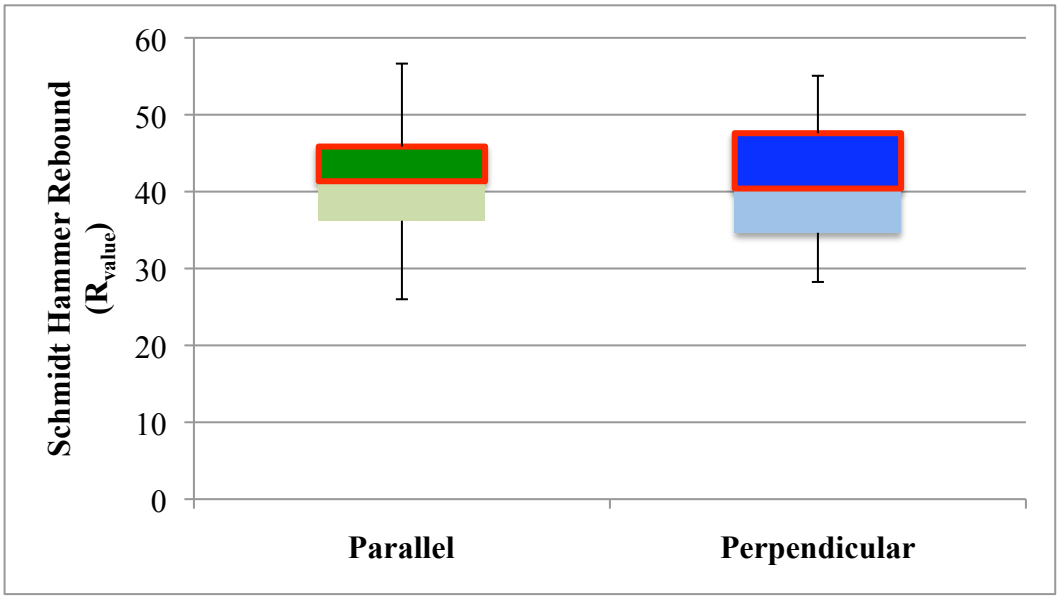

Figure 21: Schmidt Hammer rebound with respect to device orientation (parallel or perpendicular to the rock's foliation). The 3rd quartiles of the data sets are boxed in red, and their overlap in range indicates that using the Schmidt Hammer orientation with respect to foliation does not appear to affect the SHR measured.

Variations in Rock Strength Due to Weathering

To assess if and how rock strength varies with respect to degree of weathering, the Schmidt Hammer was used in four distinctly different field areas: the road cuts, Green Lakes Basin, Betasso Gulch, and Gordon Gulch.

Road Cuts

Several road exposures of different lithologies were tested with the Schmidt Hammer to quantify how rock strength varies with respect to weathering at various depths below the surface (Figure 22). The Schmidt Hammer rebound data (SHR) collected from the road cuts ranged from 13 to 61 R_{value} (Appendix D). AR1 is strongest 6.4 m below the surface (61 R_{value}), then becomes weaker (39 R_{value}) at 3.1 m below the surface; however, it then becomes stronger at the surface (45 R_{value}; Figure 23A). On the other hand, both AR2 and AR3 are weakest at the surface (14 and 19 R_{value} respectively), and increase in strength with depth (46 and 31 R_{value} at 3 m and 53 and 40 R_{value} at the farthest from the surface; Figure 23B and 23C). Therefore, the strongest SHR measurements were taken at the deepest surfaces of each road cut, an intermediate range of SHR was measured in the mid-region, and the weakest rock tends to be at the top of the road cuts (Figure 24).

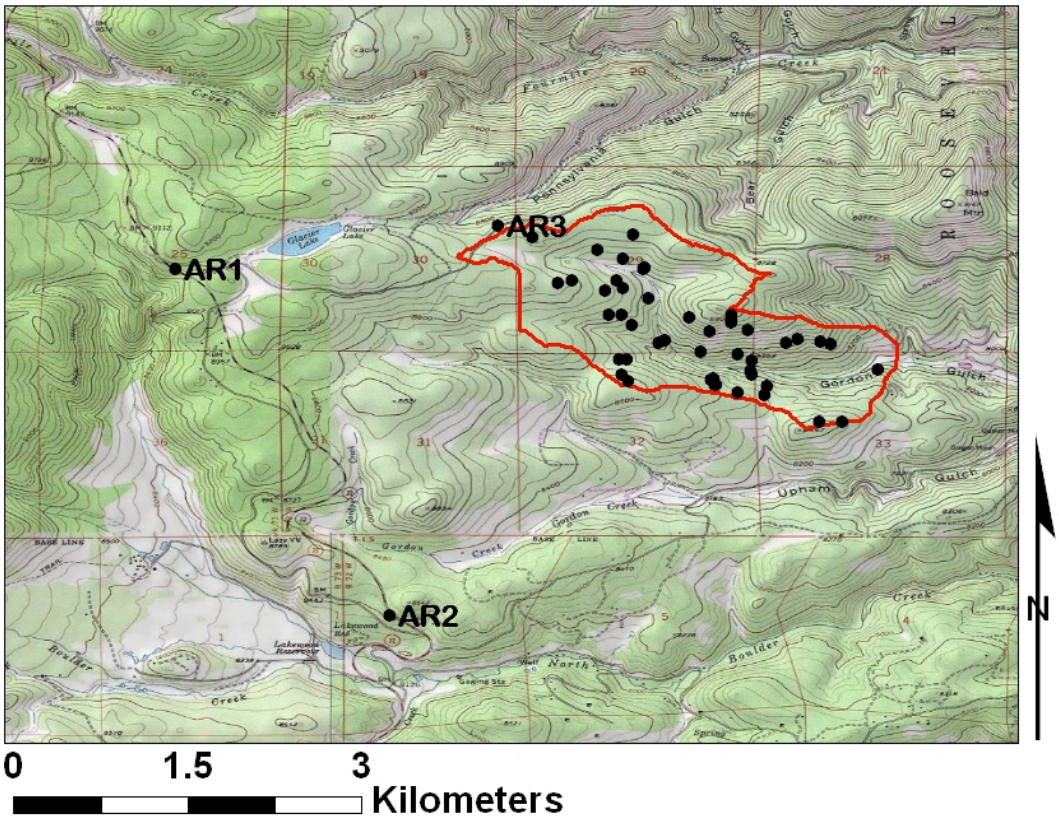

Figure 22: Map detail of the area around Gordon Gulch (outlined in red). Road exposures AR1, AR2, and AR3 are labeled.

23A.

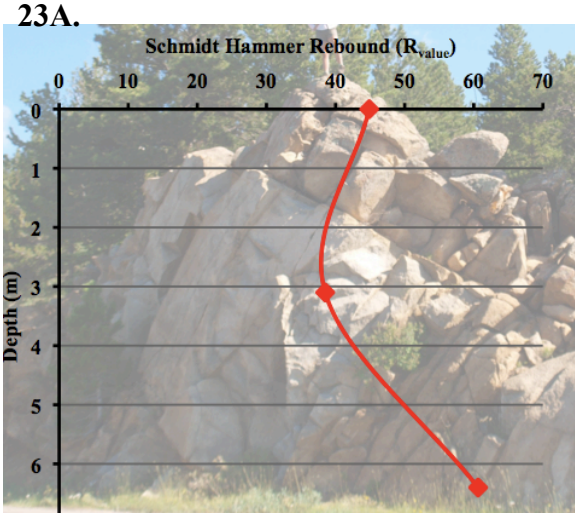

23B.

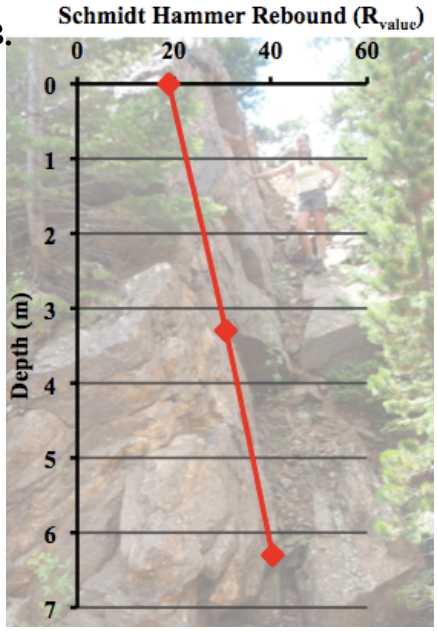

23C.

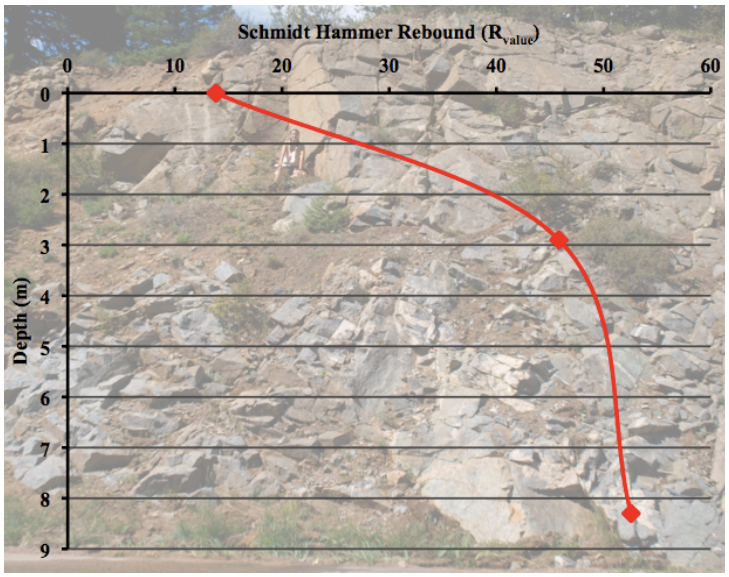

Figure 23: A. Rock strength profile of AR1. **B.** Rock strength profile of AR3. **C.** Rock strength profile of AR2.

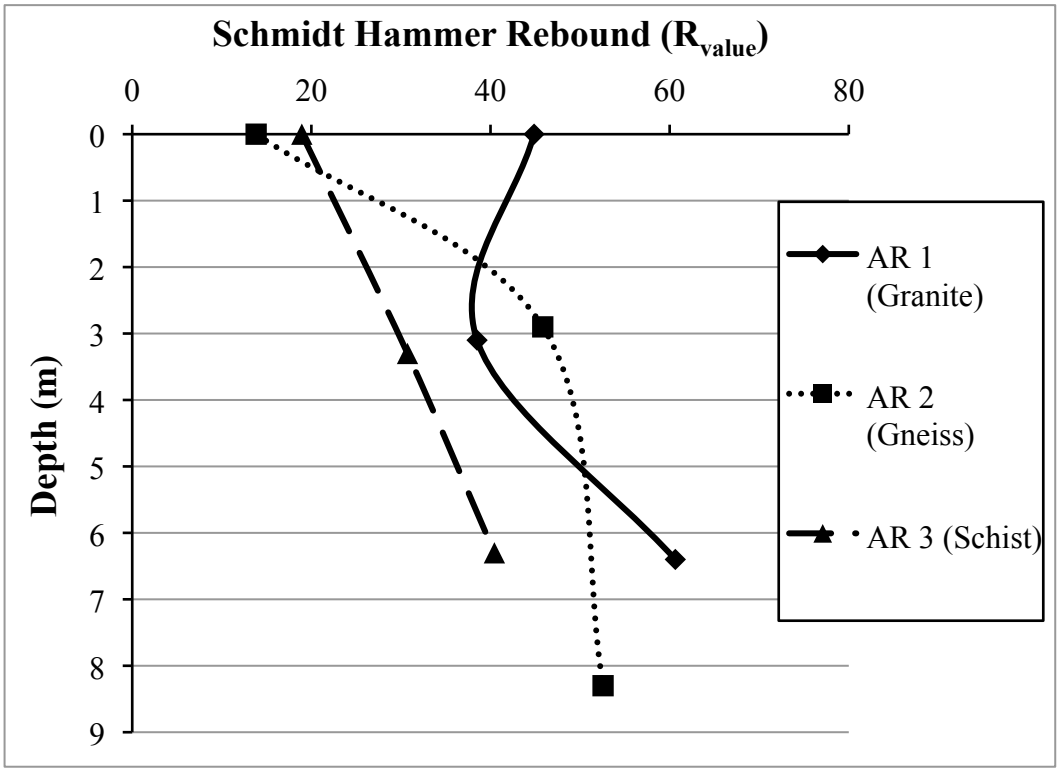

Figure 24: Schmidt Hammer rebound with respect to depth as measured from all 3 road cuts. Illustrates that rock strength increases as depth increases and weathering decreases.

Green Lakes Basin

In Green Lakes Basin, the alpine field location, weathered and polished bedrock of both metasedimentary and granitic composition were tested to assess variations in strength due to weathering and location in the valley. The Schmidt Hammer was used to test the UCS of 22 different bedrock surfaces within the basin (Figure 25). The obtained measurements of SHR ranged from 23 to 69 R_{value} (Appendix A). The mean SHR for the glacially polished bedrock was 54 R_{value}, with a 3rd quartile range from 59 to 61 R_{value}. The polished bedrock of metasedimentary composition had a mean SHR of 58 R_{value} and the granitic polished bedrock also had a mean SHR of 58 R_{value}. For the weathered bedrock, the mean SHR was 33 R_{value} and the 3rd quartile range was between 33 and 42 R_{value}. The metasedimentary weathered bedrock had a mean SHR of 23 R_{value}; whereas, the mean SHR for granitic weathered bedrock was somewhat higher at 36 R_{value}.

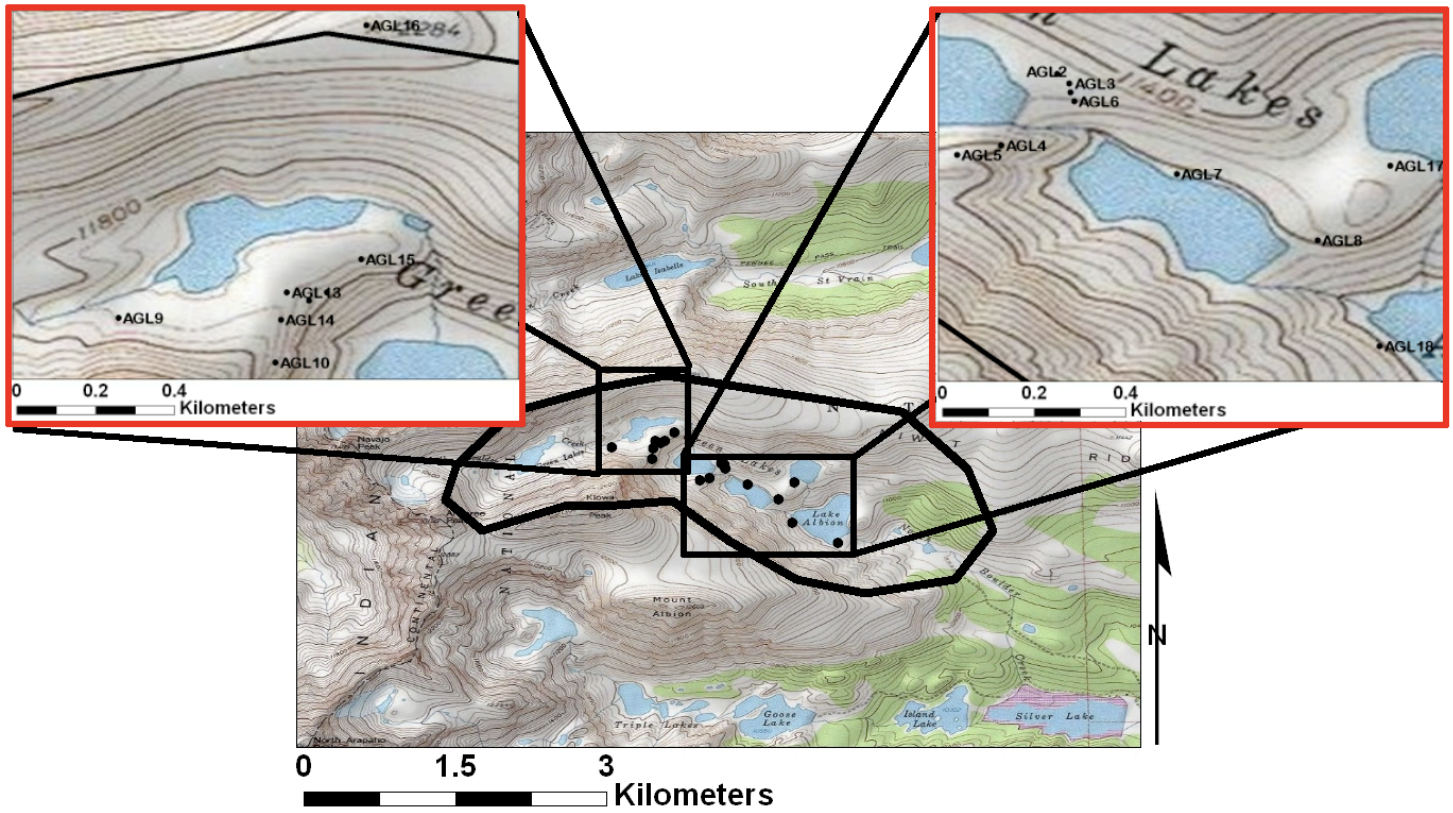

Figure 25: Map of Green Lakes Basin with insets detailing the locations of each sample site.

Bedrock of both lithologic groups were also tested in Gordon Gulch and Betasso Gulch, which are at lower elevations, to quantify variations in rock strength and weathering in catchments of a distinctly different climatic history and setting. Additionally, rock weathering was documented throughout Gordon Gulch to evaluate the role that rock strength plays in the development of hillslopes in this area.

Betasso Gulch

Twenty sites of granitic bedrock were tested with the Schmidt Hammer along Betasso Road and another five surfaces were tested at Bummer's Rock (Figure 26). In Betasso Gulch, the obtained SHR measurements spanned between 0 and 56 R_{value} (Appendix C). The mean SHR was 20 R_{value} and the 3rd quartile range was between 18 and 25 R_{value}. At Bummer's Rock, the ridge top tor in Betasso, SHR measurements ranged from 21 to 49 R_{value} and the mean SHR was 36 R_{value} and the 3rd quartile range was from 32 to 46 R_{value}.

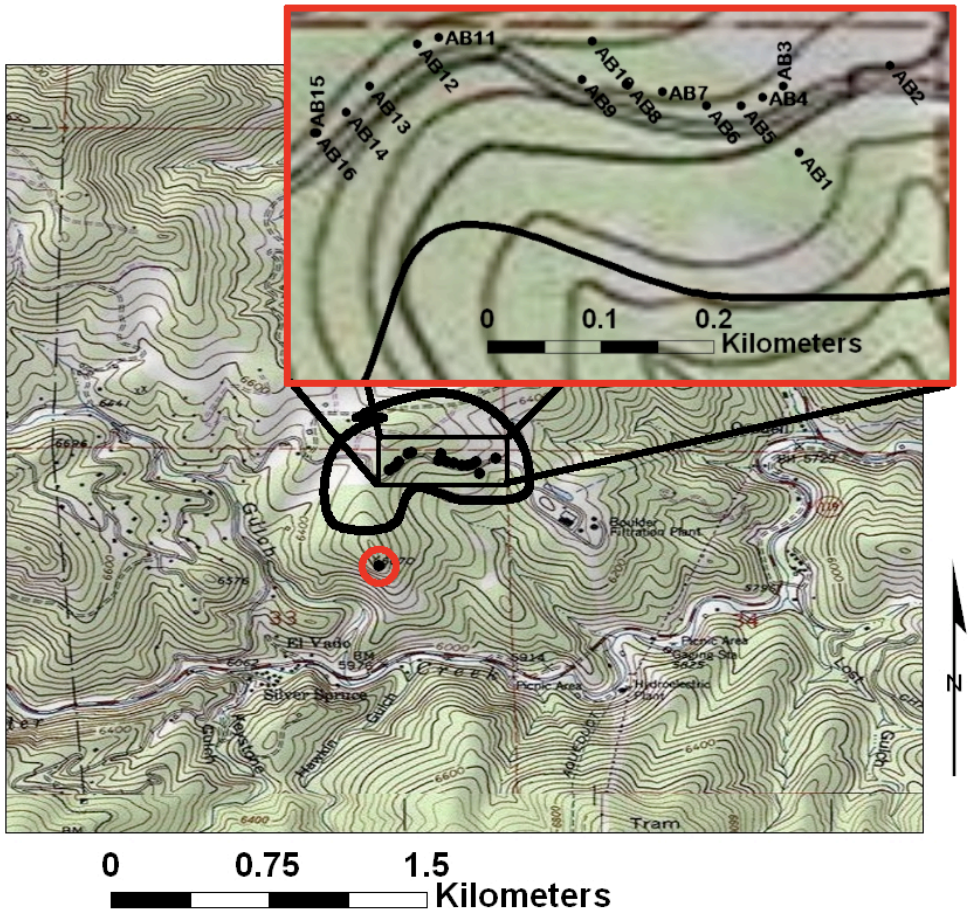

Figure 26: Map of Betasso Gulch. Inset shows study sites along Betasso Road and the red circle indicates the location of Bummer's Rock.

Gordon Gulch

In Gordon Gulch, thirty-eight tors and eight soil pits with exposed saprolite were tested with the Schmidt Hammer (Figure 27). The SHR measurements obtained ranged from 8 to 51 R_{value} (Appendix B). The tors had a mean SHR of 39 R_{value} and a 3rd quartile range of SHR between 38 and 46 R_{value}. The exposed saprolite had a significantly lower mean SHR of 21 R_{value} and the 3rd quartile ranged from 19 to 28 R_{value}.

To evaluate the differences in tor size, spacing, and location throughout Gordon Gulch, differences in both lithology and location were also assessed. Tors of metasedimentary composition had a mean SHR of 40 R_{value} and a 3rd quartile range of 40 to 44 R_{value}. Granitic tors, on the other hand, had a mean SHR of 35 R_{value} and a 3rd quartile range of 36 to 41 R_{value} (Figure 28). On the south-facing slopes, tors had a mean SHR of 40 R_{value}, with a 3rd quartile that ranged from 40 to 43 R_{value}. In contrast, the tors on the north-facing slope had a mean SHR of 33 R_{value} and a 3rd quartile range of 36 to 37 R_{value} (Figure 29), which is somewhat less than the SHR of those on the south-facing slope.

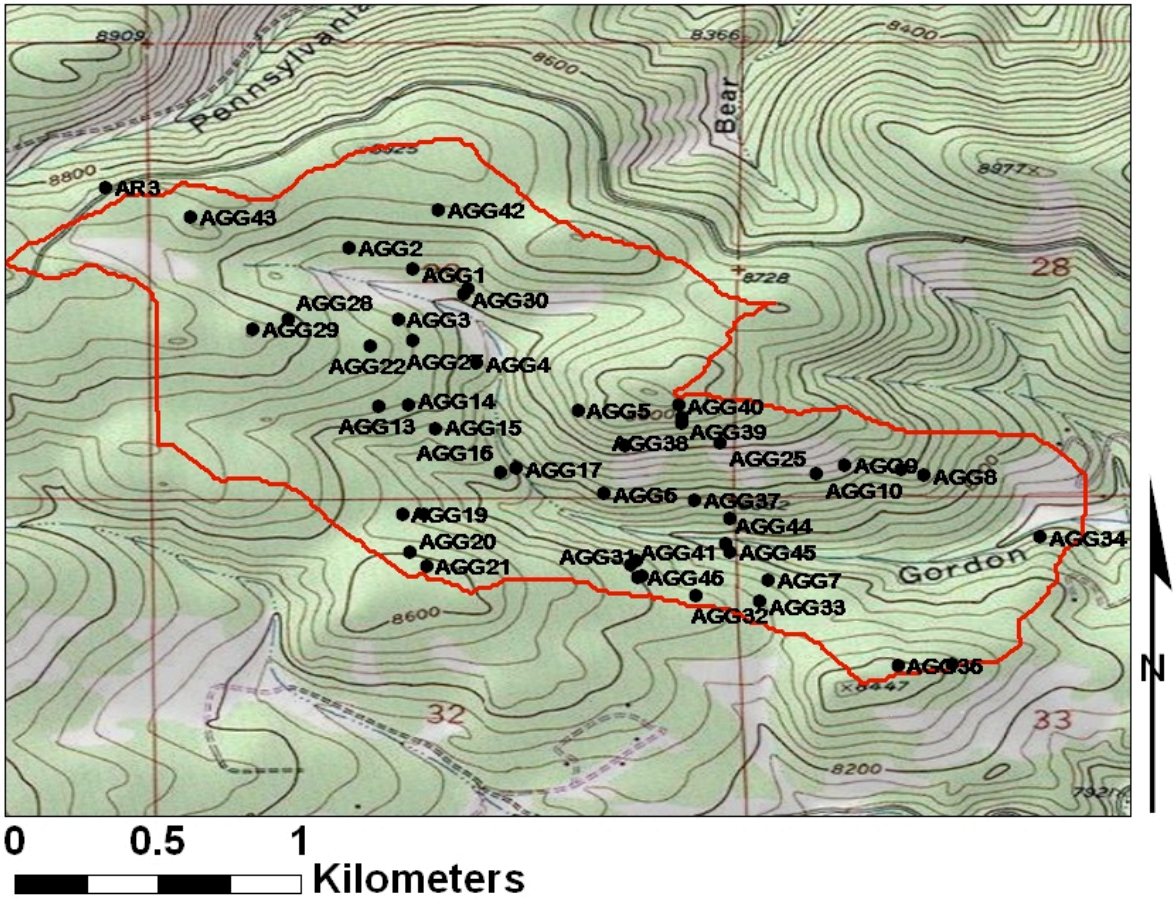

Figure 27: Map of Gordon Gulch (outlined in red). Study sites are labeled.

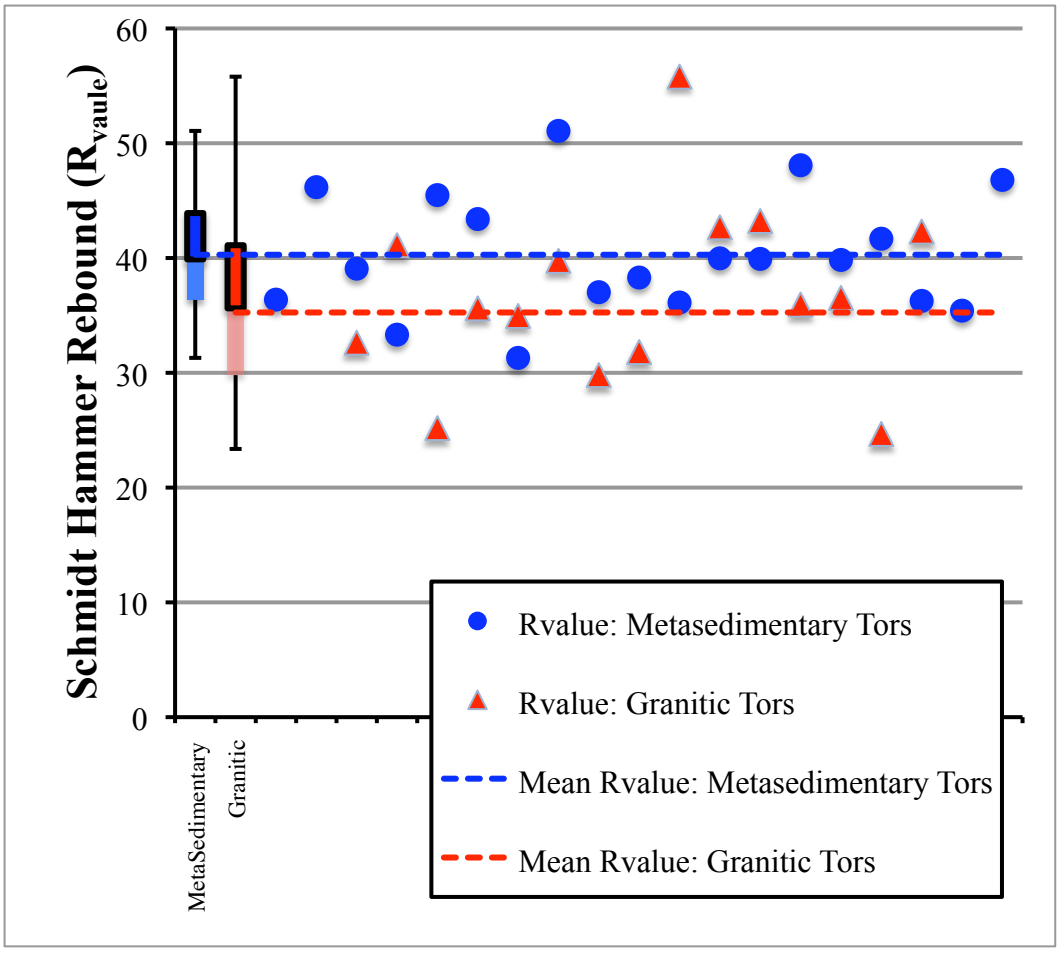

Figure 28: Schmidt Hammer Rebound measurements with respect to lithology from Gordon Gulch. Each point is representative of a tor's mean R_{value}, the dashed lines represent the mean R_{value} for a specific lithology in the gulch, and the boxes outlined in black in the box/whisker plots are the 3rd quartile of the data sets. This plot shows that metasedimentary tors are slightly stronger than granitic tors in Gordon Gulch.

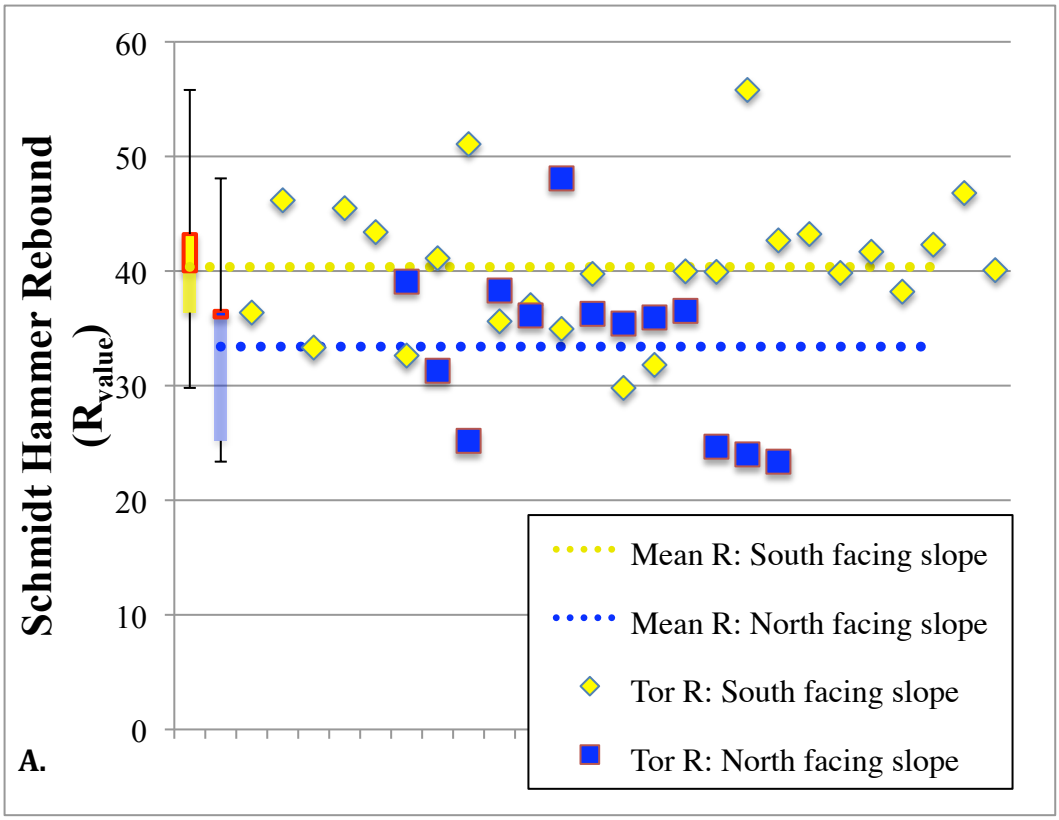

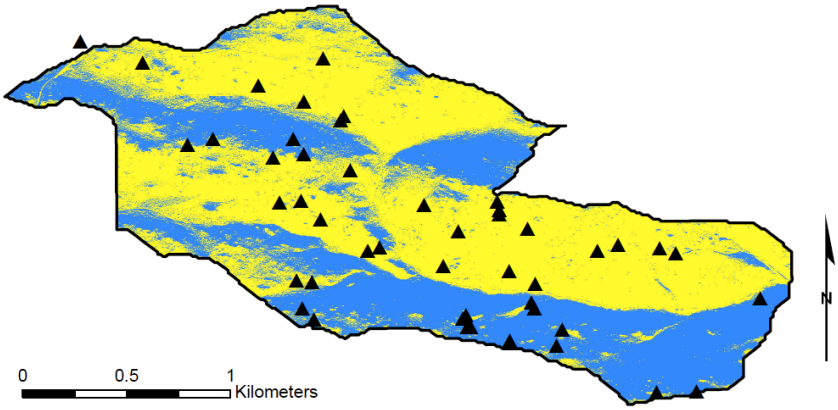

Figure 29: A. Schmidt Hammer Rebound measurements with respect to slope aspect in Gordon Gulch. Each point is representative of a tor's mean R_{value}, the dashed lines represent the mean R_{value} for tors on a specific slope in the gulch, and the boxes outlined in red in the box/whisker plots are the 3rd quartile of the data sets. This plot shows that tors on the south-facing slope are slightly stronger than those on the north-facing slope. **B.** Map of Gordon Gulch. Triangles are test sites, yellow regions represent the south-facing slopes and the blue regions are the north-facing slopes.

To investigate how rock varies on individual tors, thirty-four tors in Gordon Gulch were tested on three surfaces: the up-slope side of the tor, the top, and the down-slope side (Figure 30). The mean SHR for the tops of the tors was 36 R_{value}, and the 3rd quartile range was between 36 and 44 R_{value}. The mean SHR value for the up-slope sides was 37 R_{value} and ranged from only 36 to 39 R_{value}. On the down-slope sides of the tors, the mean SHR was 43 R_{value} and the 3rd quartile ranged from 41 to 48 R_{value}. To ascertain whether or not trends in rock strength on various faces of the tor was related to rock type, each lithologic group was then assessed separately (Figure 31). For tors of metasedimentary composition, the up-slope faces had a 3rd quartile range of 38 to 43 R_{value}, the top faces ranged from 36 to 44 R_{value}, and the down-slope faces from 46 to 52 R_{value}. Granitic tors had a 3rd quartile range of 30 to 36 R_{value} on the up-slope faces, 29 to 36 R_{value} on the top faces, and 40 to 44 R_{value} on the down-slope faces.

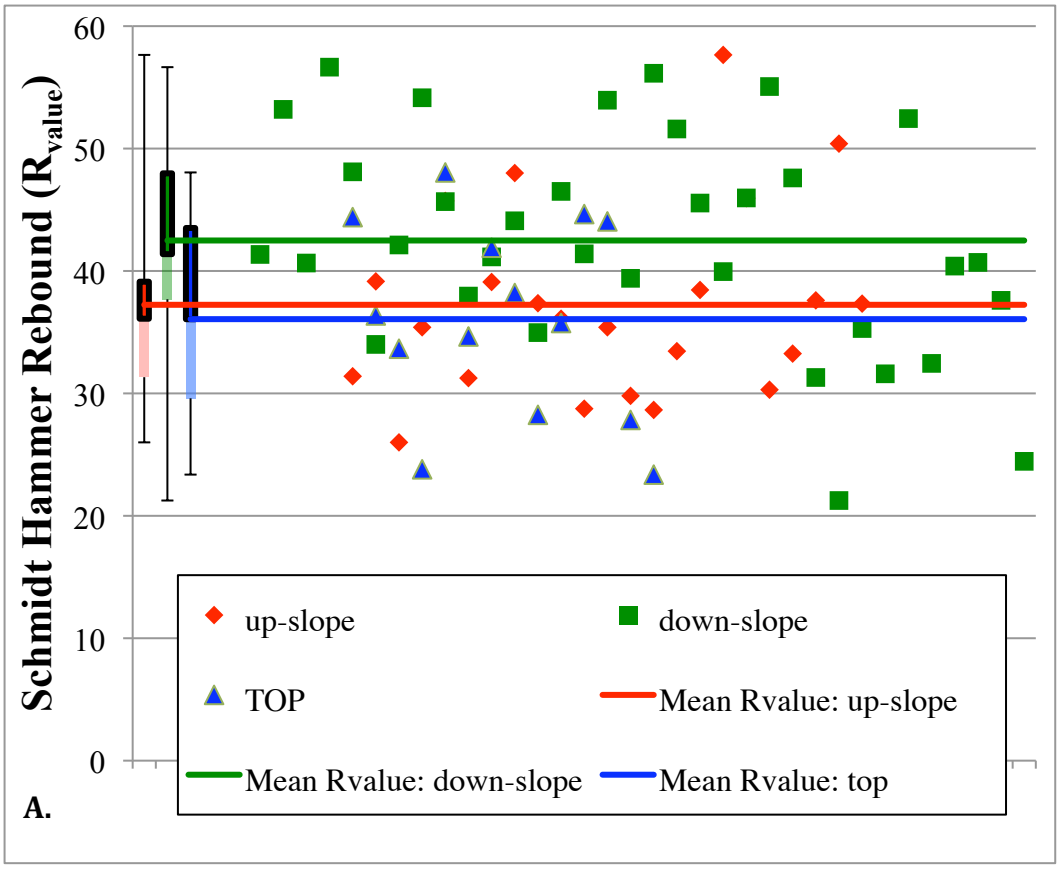

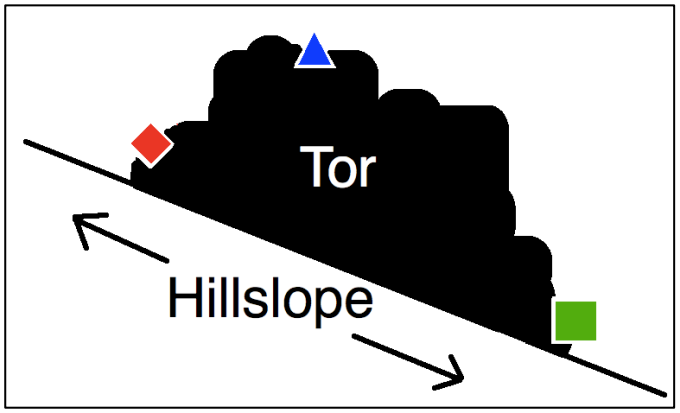

Figure 30: A. Schmidt Hammer Rebound with respect to the tor face tested. Each point is representative of a tor's mean R_{value} on a given face, the horizontal lines represent the mean R_{value} for a specific tor face, and the boxes outlined in black in the box/whisker plots are the 3rd quartile of the data sets. This plot shows that down-slope face of a tor is slightly stronger than the up-slope face, which in turn is slightly stronger than the top. **B.** Schematic of a tor on a hillslope, symbols for up-slope, down-slope, and top faces correspond with the legend in **A**.

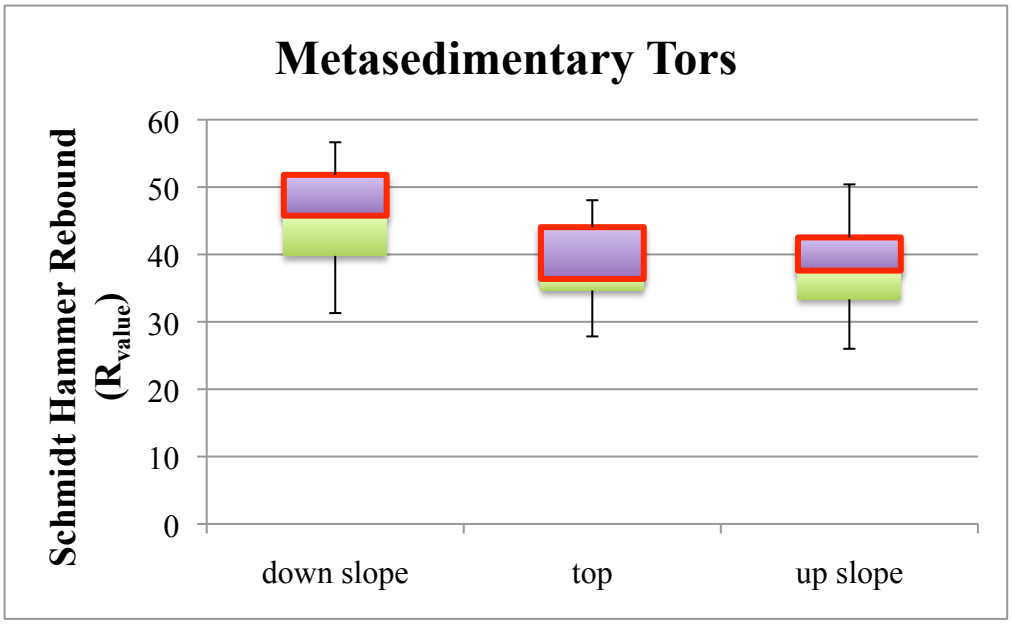

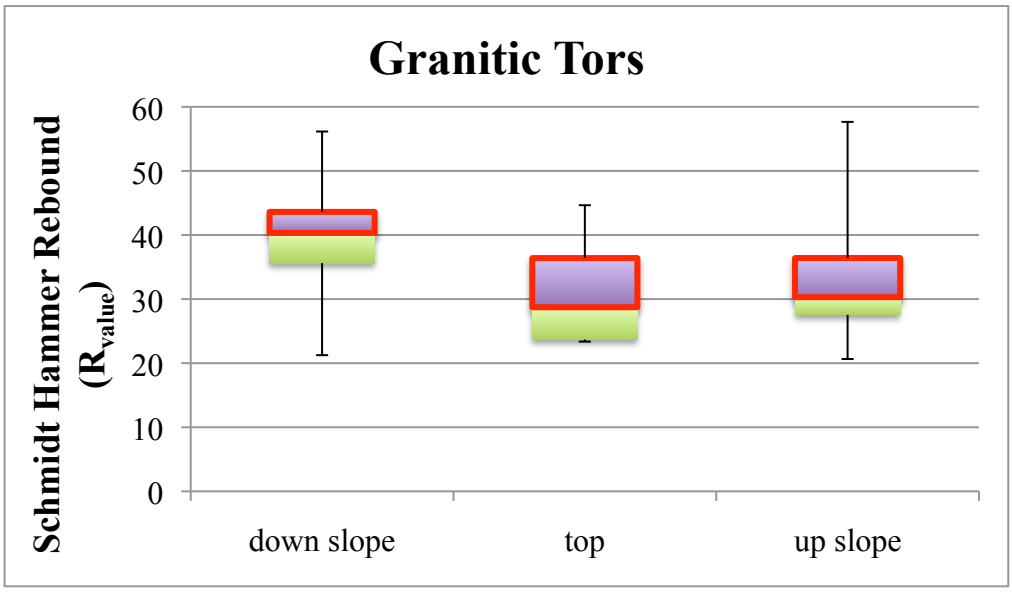

Figure 31: Box/whisker plots of Schmidt Hammer Rebound with respect to location tested on the tor, with tors of metasedimentary composition in the top graph and tors of granitic composition in the lower graph. The 3rd quartile of each data set is boxed in red. Together, these plots show that the location on the tor matters more in determining compressive strength than lithology.

Distance Between Fractures / Fracture Density

Tors in Gordon Gulch

In order to better understand the controls on tor size and location in Gordon Gulch, the density of fracture spacing on tors was considered. The distance between fractures was measured along forty-four different faces of thirty-two tors in Gordon Gulch. The average space between fractures in the tors ranged from 10 to 100 cm (Appendix B). Fracture spacing shows a small variation between the north- and south-facing slopes of the gulch. On the south-facing slope, the mean space between fractures was 10 cm wider than on the north-facing slope. Another way to compare the fracture characteristics is to assess the distribution frequency of the distance between fractures. When frequency is compared across the gulch, tors on the north-facing slope have a higher occurrence of more closely spaced fractures than tors on the south-facing slope, which have a higher occurrence of slightly wider spaced fractures (Figure 32).

Saprolite in Betasso Gulch

Fracture spacing was also measured in Betasso Gulch to further evaluate the impact of fractures on rock strength and weathering. Measurements were taken along eight different sections of saprolite outcrop along Betasso Road. The average space between saprolite fractures in Betasso Gulch range from 6 to 33cm and the mean space between fractures in the saprolite is 13 cm (Appendix C).

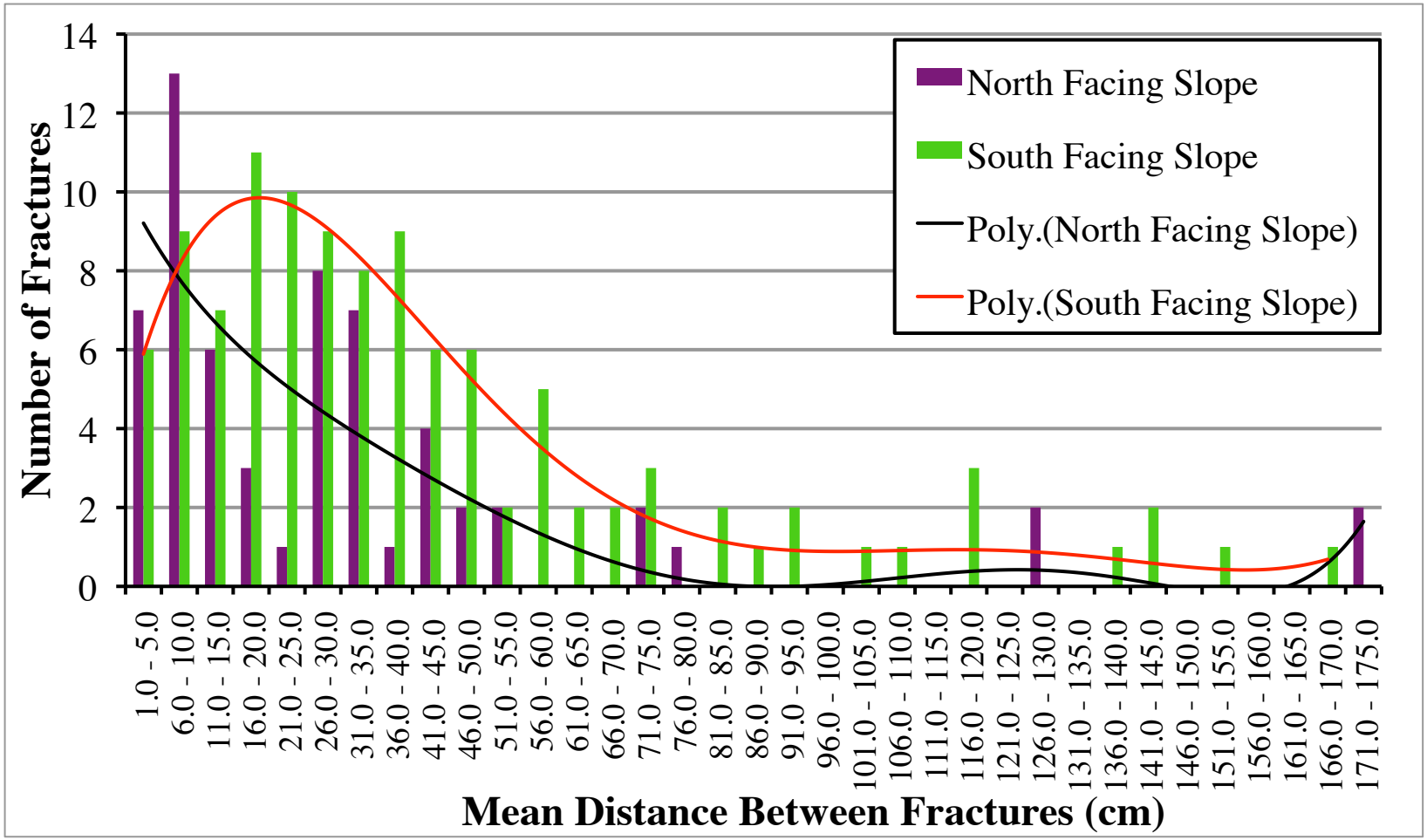

Figure 32: Number of Fractures with respect to the Mean Distance Between Fractures. The best fit lines help illustrate that there are more closely spaced fractures on the north-facing slope and more widely spaced fractures on the south-facing slope.

Fracture and Foliation Orientation

Fracture orientation was measured on a total of one hundred and eighty-one fractures in the same thirty-two tors measured for fracture spacing in Gordon Gulch. The fractures do not display a strong preferential orientation, but most have moderate dip (around 30°-40°; Figure 33). Foliation orientation was measured from twenty different locations on ten different tors in Gordon Gulch. The foliation of the metasedimentary rocks have a preferred orientation, which is, on average, 281°/ 48° NE (Figure 34).

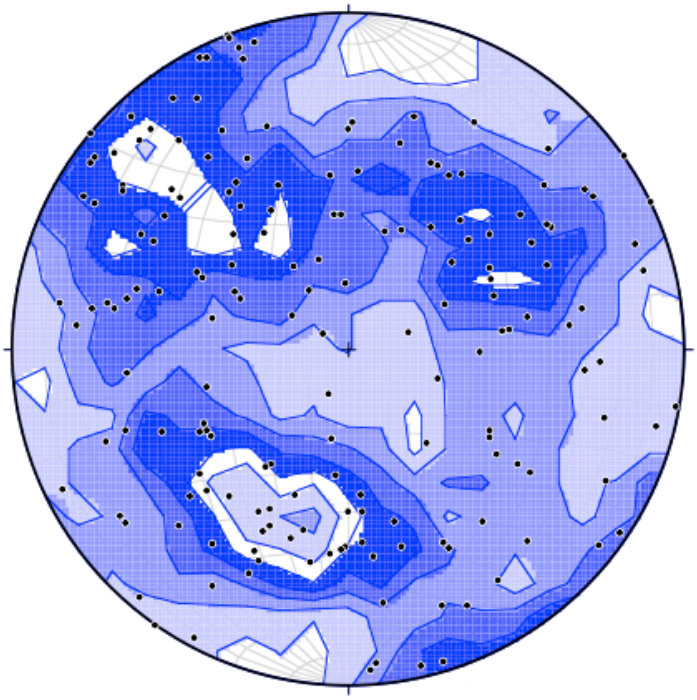

Figure 33: Stereographic projection of the poles to planes of one hundred and eighty-one measured fracture orientations from tors in Gordon Gulch. Although there does not appear to be a strong preferred fracture orientation, there is a cluster of poles in the south-western hemisphere that represent fractures along foliation planes. (Contour Interval = 1sigma)

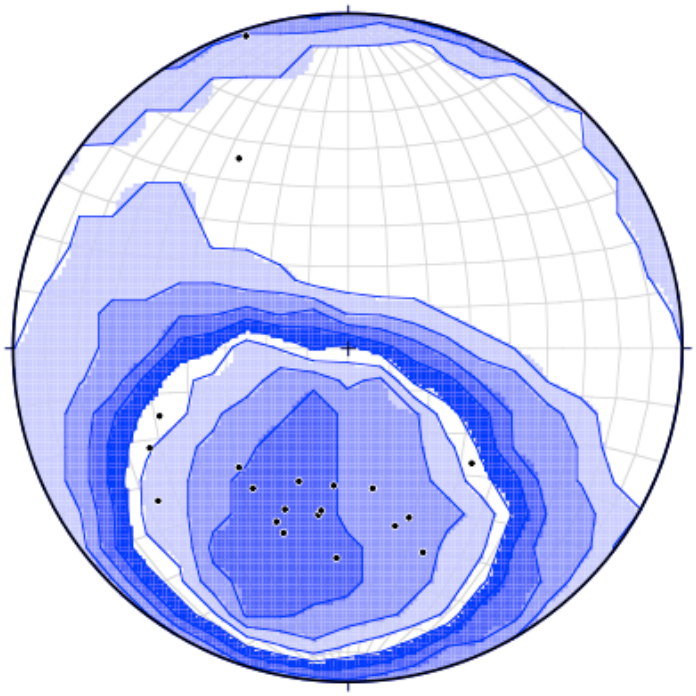

Figure 34: Stereographic projection of the poles to planes measured in Gordon Gulch from twenty different foliations in metasedimentary tors. The preferred orientation of the foliation is, on average, 281°/48° NE. (Contour Interval = 1sigma)

INTERPRETATIONS

The Influence of Lithology on Rock Strength

Bedrock of both metasedimentary and granitic composition was tested with the Schmidt Hammer to assess the relationship between rock strength and lithology. When the Schmidt Hammer rebound (SHR) measurements from both weathered and unweathered bedrock were compared by lithology, both yielded a distribution of measurements that seem essentially comparable. However, weathered bedrock tors from Gordon Gulch show a different relationship between rock strength and lithology. While the upper and lower limits of the granitic and metasedimentary groups overlap by 2 R_{value} units, the mean SHR of the two groups differ by 7 R_{value} units. Therefore, in Gordon Gulch it appears that the metasedimentary bedrock is slightly stronger than the granitic bedrock.

The laboratory testing of uniaxial compressive strength (UCS) shows a similar result as the SHR data from Gordon Gulch. In the laboratory, the fresh/unweathered metasedimentary bedrock samples tested were approximately 70 MPa stronger than fresh/unweathered granitic bedrock samples. Since the

laboratory results demonstrate that the fresh metasedimentary rock is slightly stronger than fresh granitic rock, as do the SHR measurements of weathered rock from Gordon Gulch; then, despite the compilation of SHR measurements that show both lithologies to be comparable, the metasedimentary rock in the Front Range is slightly stronger than the granitic rock.

It is worth noting that the SHR measurements were not dampened by the orientation of the Schmidt Hammer with respect to foliation in the metasedimentary rock. Because the 3rd quartile range of SHR for measurements taken both parallel and perpendicular to the foliation overlap almost entirely, and the mean SHR values are the same for both orientations, the presence of foliations does not appear to influence the Schmidt Hammer's measurements of rock strength for this group of metasedimentary rocks. This interpretation could either mean that the Schmidt Hammer is not sensitive enough to reflect a difference in strength between orientations, or that this group of metasedimentary rock is very cohesive, even across foliation.

Rock Strength with Respect to Weathering Across a Landscape

When the SHR data from all field locations are compiled, three distinct groupings of similar SHR can be seen (Figure 35). These are, in descending order of SHR, the glacially polished bedrock from Green Lakes Basin, the tors and weathered Green Lakes bedrock, and the saprolite.

The glacially polished bedrock from Green Lakes Basin has the highest SHR, with a 3rd quartile range between 59 and 61 R_{value}. Since this group of rock has retained its glacial polish, it can be inferred that it has not experienced extensive surface weathering, which visually makes it the least weathered surface across the landscape. However, since the polished alpine bedrock surfaces also have the highest SHR measurements, it then follows that surfaces that are the least weathered are also the strongest.

The second grouping of similar SHR is made up of the tors from Gordon Gulch and Bummer's Rock, as well as the weathered alpine bedrock from Green Lakes Basin. The two groups of tors have overlapping 3rd quartile ranges of 38 to 46 R_{value} in Gordon Gulch and 21 to 49 R_{value} at Bummer's Rock, which makes them comparable in strength and degree of weathering. This inference is logical since both groups of tors would have undergone similar weathering processes in the course of their formation. Furthermore, it is fitting that these tor surfaces have lower SHR measurements than the polished bedrock in Green Lakes Basin, since the tors have experienced weathering during formation and the polished alpine bedrock has avoided extensive surface weathering. However, the weathered bedrock from Green Lakes Basin also has a 3rd quartile range comparable to that of the tors (33 and 42 R_{value}). Given that these weathered alpine surfaces have not developed into tors, and that they are immediately adjacent to polished alpine bedrock that is much stronger, their lower UCS measurements warrant more careful consideration.

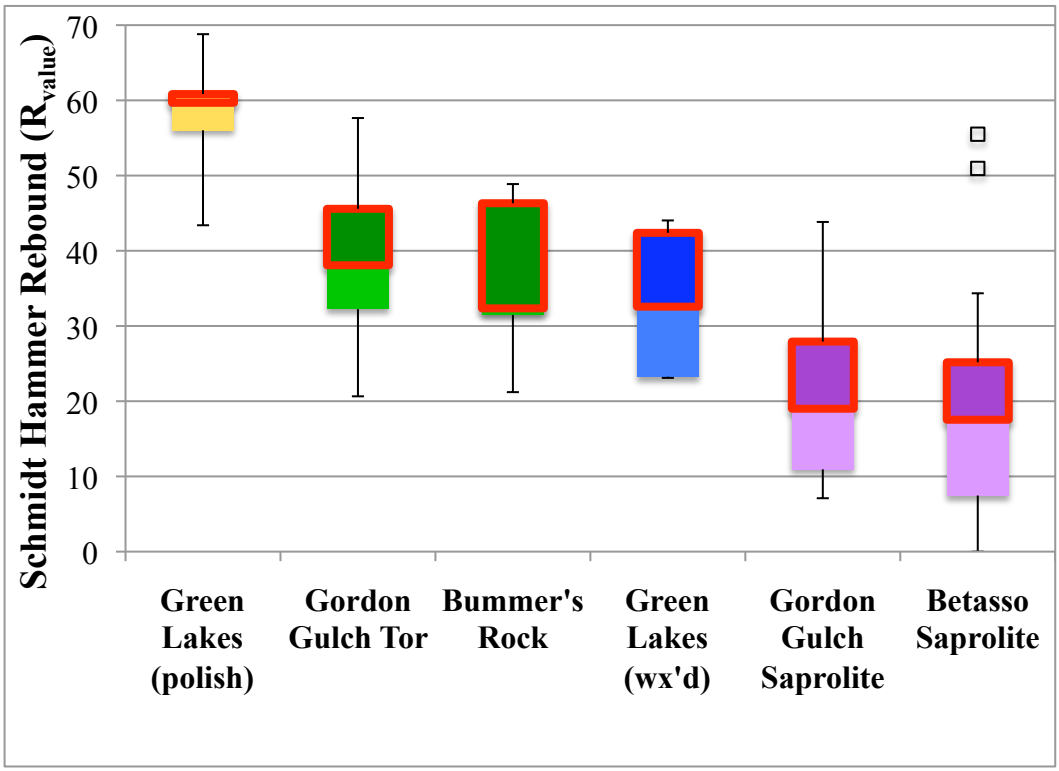

Figure 35: Box/whisker plots from each of the primary field locations. The third quartile of each data set is boxed in red. Three distinct groupings of rock strength are apparent: the polished Green Lakes bedrock, Gordon Gulch tors / Bummer's Rock / weathered Green Lakes Bedrock, and Gordon Gulch Saprolite / Betasso Saprolite. Therefore, rock strength is highest in fresh/unweathered rock, drops to an intermediate range of strength once it weathers, and with increased weathering reduces to a very low compressive strength.

One potential rationalization is that after the last glacial retreat (~15 ka) an amount of sediment covered some of the bedrock, and the surfaces that have maintained their polish until the present were among those areas covered until only recently when the sediment has been removed, exposing them to surficial weathering. This would also mean that the adjacent weathered bedrock was most likely uncovered and exposed to the surface for much longer, allowing weathering processes at the surface to remove any polish that may or may not have been present, and reduce the compressive strength of the surface. Alternatively, a variance in mineralogy across the bedrock may have allowed one area to experience more effective surficial weathering than another, or some surfaces may have never become polished to begin with. Whatever the cause, the SHR relationship between the glacially polished and weathered alpine bedrock demonstrates that once bedrock weathers, its strength drops from a high value, such as that of the glacially polished bedrock in Green Lakes Basin, to a lower, intermediate grade of compressive strength, such as the weathered alpine bedrock and the tors. Furthermore, since both the tors and the weathered alpine bedrock have similar SHR measurements, it could be presumed that a drop in rock strength with weathering is not directly correlated with site-specific weathering, but rather with the nature of how the rocks themselves deteriorate.

But the story that can be constructed from the data presented in Figure 35 does not end with the weathering of bedrock to an intermediate grade of compressive strength. Rather, it shows that when physical and chemical

weathering persist, and bedrock degrades to saprolite, the strength of the material is reduced even farther to the lowest material strength found across the landscape. This is demonstrated by the comparable SHR measurements of the saprolite in both Gordon Gulch and Betasso Gulch, with 3rd quartile ranges of 19 to 28 R_{value} and 18 to 25 R_{value} respectively.

However, while these two groups of saprolite seem very similar in compressive strength, there are two outliers in the Betasso Gulch data set (depicted as boxed points in Figure 35) that represent rock surfaces of significantly higher SHR measurements. Further investigation into the sources of these anomalous data points revealed that they are actually representative of two pegmatite veins that were tested in the Betasso Gulch field area. Their maintained strength, in spite of the extensive weathering that has deteriorated the surrounding rock, is most likely due to their different textural and mineralogical compositions. Therefore, despite the anomalous data points, the saprolite in both Gordon Gulch and Betasso Gulch is representative of the weakest, most weathered rock across the landscape.

Rock Strength with Respect to Depth and Weathering

The road cuts examined in the field provided an excellent opportunity to determine if a gradient in rock strength exists down an exposed profile of the subsurface. Figure 24 demonstrates that there is in fact a correlation with depth

below the "surface" (top of the road cut) and rock strength/ the SHR measurement. At both AR2 and AR3, the surface SHR measurements are between 10 and 20 R_{value}, which means that at 0 m depth the strength of the bedrock is lower than at any of the other areas tested at the road cuts.[8] At approximately 3 m depth below the surface, the bedrock at all three road cuts dropped down to between about 30 and 45 R_{value}. This drop in SHR with increased depth from the surface is interpreted to signify that less weathering has influenced the bedrock 3m below the surface in comparison to the rock at 0 m depth. Furthermore, at the farthest depths measured, between 6.5 and 8.5 m below the surface, SHR measurements were slightly higher, between 35 and 60 R_{value}. The slight increase in SHR from 3 m depth to 6.5 to 8.5 m depth is not as drastic or distinct as the increase in strength from 0 m to 3 m, however, the SHR measured at all 3 road cuts does increase at least marginally with depth, and is significantly higher at the lowest points of the exposures, supporting the relationship between increased depth, decreased effects of weathering, and increased rock strength.

Furthermore, when the SHR measurements from the tops, middles, and bottoms of the road cuts are averaged, the mean R_{value} for each zone of road cut is comparable to one of the three groups of weathering seen across the landscape as a whole (Table 2). The deepest bedrock at the road cuts have a mean SHR of 50

[8] AR1 has a much higher UCS at the surface than the other road cuts; however, AR1 appears to resemble a tor that has been cut through rather than continuous bedrock. Therefore, since the tops of tors have similar UCS as the side faces it is logical that the surface UCS measurement at AR1 would be comparable to UCS measurements throughout the road cut.

R_{value}, which is similar to that of the strongest rock across the landscape, the glacially polished bedrock in Green Lakes Basin, that has a mean of 54 R_{value}. Likewise, the bedrock from the middle of the road cuts has a mean strength quantified as 38 R_{value}, which is similar to the measurements of the tors and weathered alpine bedrock of 36, 39, and 33 R_{value} respectively. Lastly, the bedrock from the tops of the road cuts was measured to be 15 R_{value} on average, which is similar to the saprolite means of 20 and 21 R_{value}. The correlation between data from the road cuts with the data from across the landscape shows that the relationship between gradients of decreased rock strength with increased weathering is not only a surface phenomenon, but also a characteristic of how rock weathers.

Table 2: The mean Schmidt Hammer R_{values} for each field location. Cells are color coded to correspond with Figure 35, and therefore separate out into three groups of UCS: the polished Green Lakes bedrock and deepest road cuts rock, the tors, weathered Green Lakes bedrock and mid-depth road cut rock, and the saprolite and most shallow road cut rock.

	Green Lakes (Polish)	*Road Cuts* (depth=6.5-8.5m)	Gordon Gulch TOR	*Road Cuts* (depth=3m)	Bummer's Rock	Green Lakes (Wx'd)	Gordon Gulch Saprolite	Betasso Gulch Saprolite	*Road Cuts* (depth=0m)
N	20	3	84	3	5	4	11	20	2
Mean Schmidt Hammer R-value	54	50	39	38	36	33	21	20	15

Rock Strength and Weathering within a Catchment

In Gordon Gulch, the exposures of bedrock at the surface come in the form of tors. Since the distribution of tors throughout the catchment is not homogeneous from one hillslope to the other, their physical characteristics were compared from one hillslope to the other. The tors on the south-facing slopes have a mean SHR of 40 R_{value} and a 3rd quartile range of 40 to 43 R_{value}; whereas, the tors on the north-facing slopes have a mean SHR of 33 R_{value} and a 3rd quartile range of 36 to 37 R_{value}. There is one tor on the north-facing slope that had an anomalously high R_{value}, which may be due to its metasedimentary lithology, since the metasedimentary bedrock has been shown to be slightly stronger. However, overall the SHR of tors on the south-facing slopes are slightly stronger than those on the north-facing slopes.

Fracture spacing could also be considered in a comparison of the physical characteristics and weathering differences between the north- and south-facing hillslopes in Gordon Gulch. On the south-facing slope, the mean distance between fractures was 10 cm wider than on the north-facing slope. Furthermore, tors on the north-facing slope have a higher occurrence of more closely spaced fractures than tors on the south-facing slope, which have a higher occurrence of slightly wider spaced fractures.

Given that tors on the south-facing slopes have greater distances between fractures and can also be characterized as having high measurements of rock

strength, SHR was assessed with respect to mean distance between fractures to evaluate the relationship between both physical characteristics (Figure 36). The primary hypothesis being tested in the comparison of these two physical characteristics is that increased fracture density would, in theory, dampen/lower SHR values since fractures provide a threshold in which the energy introduced to the test material from the Schmidt Hammer's impact can be absorbed. However, for tors in Gordon Gulch, the nearly horizontal slope of the linear trend line shows that there is not a strong correlation between SHR and distance between fractures; therefore, fracture density does not independently influence measured rock strength. However, when SHR is evaluated with respect to mean distance between fractures in saprolite from Betasso Gulch, the linear trend line shows a steep, positive correlation between the two physical characteristics. For this reason it could be interpreted that the distance between fractures could directly influence SHR in saprolite. It is critical, however, to make note that 50% of the mean fracture spacing measurements for the saprolite are lower than any of the distance measurements from the tors. Thus, instead of rationalizing that fracture spacing influences SHR in saprolite and not in tors, it may be more accurate to deduce that fracture spacing on the order of 10 cm or less may affect SHR while greater distances between fractures do not.

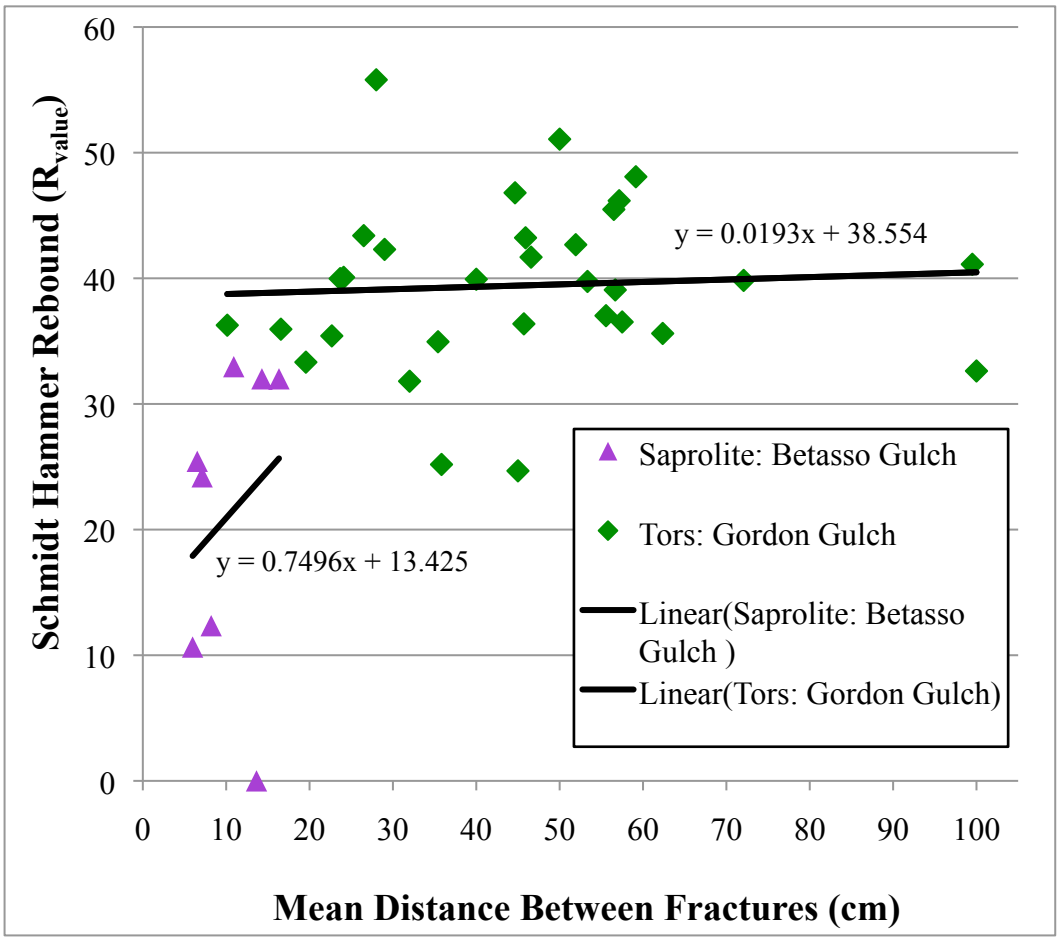

Figure 36: Schmidt Hammer rebound (SHR) with respect to mean distance between fractures. Green diamonds plot for tors in Gordon Gulch and purple triangles show saprolite in Betasso Gulch. Linear best-fit lines are plotted for each. While fracture spacing and SHR may be directly proportional in saprolite, there is not a strong correlation between them with respect to tors.

In an effort to more fully comprehend how tors behave and evolve in a hillslope setting, the up-slope, down-slope and top sides of tors in Gordon Gulch were distinguished and measured separately. While the 3rd quartiles of the SHR measurements for the tops of the tors overlap with both the down-slope and up-slope faces by 3 units of R_{value}, the up-slope and down-slope faces are distinctly different, with a gap of 6 units of R_{value} between their respective mean SHR values and 2 units of R_{value} between their respective 3rd quartile ranges. Therefore, given the overlapping 3rd quartile ranges, the strength ratings around a tor, from strongest to weakest, are the down-slope faces, the tops, and lastly the up-slope faces; which is a trend that is seen in both metasedimentary and granitic tors. This seems rather anomalous, since this study assumed that the tops of the tors would actually be the weakest, as they would have gone through the "feed-through reactor" that is the critical zone before the lower areas of the outcrop and therefore would have experienced a greater amount of weathering. This hypothesis is also challenged because it postulates that both the down-slope *and* up-slope sides should be stronger than the tops, since they are "lower" in the "feed-through reactor;" and yet, while the down-slope sides are slightly stronger than the top faces, the up-slope sides are weaker. Therefore, the weathering gradient of a tor, from a more weathered top to less weathered lower sides, presented by Linton (1955), is either inaccurate or needs to be significantly modified for tors in a hillslope setting.

DISCUSSION

Bedrock weathering is a crucial element of landscape morphology, and to fully understand how hillslopes develop it is imperative that geomorphologists continue to cultivate and enrich their understanding of how bedrock weathers. By quantifying weathering and other physical characteristics of bedrock with the concept of rock strength, this project aims to better inform landscape evolution models. This study provides a broad context for how rock strength changes across a landscape with respect to variations in weathering and depth below the surface; however, the weathered and polished alpine surfaces, as well as the tors and saprolite at lower elevation, still merit further scrutiny of how such physically different bedrock has developed within such close proximity.

Rock Strength Differences Between Adjacent Bedrock

Green Lakes Basin

In Green Lakes Basin, fresh, glacially polished bedrock of high compressive strength and weathered bedrock of much lower strengths can occur within a meter of each other. As previously explained, one potential rationalization for this contrast in rock strength is that after de-glaciation sediment covered areas of bedrock, protected the glacially polished surfaces until it was recently removed. However, cosmogenic ^{10}Be dating of glacially polished surfaces in Green Lakes Basin has shown that they have been exposed at the surface since de-glaciation (Dühnforth and Anderson, 2011). Therefore, sediment coverage could not have acted as a barrier protecting these surfaces from weathering.

Alternatively, a variance in mineralogy across the bedrock may have allowed one area to experience more effective surficial weathering than another (e.g. an increase in modal % of biotite, a mineral that experiences more intense expansion during freeze/thaw cycles), or some surfaces may have never become polished during glaciation, which may have promoted subsequent mechanical and chemical weathering. As such, it appears that the original state (polished or weathered) of the bedrock may significantly influence the rate and degree of observed rock weathering. One implication of this conclusion affects the use of rock weathering for relative surface exposure ages because it demonstrates that

rocks of similar exposure ages do not necessarily have the same strength; and furthermore, that rocks with different exposure histories can appear comparable in strength. The relationship of Schmidt Hammer rebound (SHR) between the glacially polished and weathered alpine bedrock of the same exposure age also demonstrates that once bedrock weathers, its compressive strength drops from a high value, such as that of the glacially polished bedrock in Green Lakes Basin, to a lower, intermediate strength, such as the weathered alpine bedrock and the tors.

Gordon Gulch

Another example of differential weathering in a small geographic area is that of the strong tors relative to the weaker, adjacent saprolite in Gordon Gulch. Here, the geomorphic processes governing the development of tors may help clarify the vastly different SHR values that characterize the adjacent bedrock exposures.

Tor Weathering on the North- and South-Facing Slopes

Tors develop where fractures and jointing are less dense, wherein denser fracturing in adjacent areas facilitates greater weathering (Twidale, 1990). In Gordon Gulch, tors are likely representative of pockets of less densely spaced fractures relative to adjacent regions where the distance between fractures may have been less. In those adjacent areas of more closely spaced fracturing, weathering processes are more likely to be effective, since a higher fracture

density can result in increased surface area for chemical weathering (Fookes et al., 1971). Ultimately, areas of higher fracture density would develop into saprolite, and adjacent regions that are less densely fractured would become tors, which is how bedrock of such different strengths can be found immediately adjacent.

A further complexity that this study has shown is that SHR is not directly related to mean distance between fractures in tors, in spite of previous concepts such as the GSI (geologic strength index), which rely on a direct correlation between fracture characteristics and rock strength (Hoek et al., 1998). In this case, the concepts of tor development may reveal a connection between higher SHR values and greater distance between fractures in tors that corresponds more closely with the relationship discussed in Fookes et al. (1971).

In the tor development model, the primary drivers in the system are chemical and physical weathering along fracture surfaces (Linton, 1955). If there are more fractures inherently in the bedrock, then, theoretically, there is more surface area that can experience the effects of weathering, especially chemical weathering (Mabee and Hardcastle, 1997; Ehlen and Wohl, 2002; Molnar et al., 2007; Moore et al., 2009). Therefore, if fracture density is lower on the south-facing slopes, then there is likely to be reduced surface area over which weathering processes can act. Also, because this study has already shown that the Schmidt Hammer can detect variance in degree of weathering in outcrop and across a landscape, perhaps the higher SHR values on the south-facing slopes

reflect a lower amount of chemical weathering on those tors due to a lower fracture density.

On the other hand, fracture density may be more closely related to observations in the variability of tor size throughout Gordon Gulch. As noted by Trotta in 2010, there are, on average, larger tors on the south-facings slopes than on the north-facing slopes. Again, because fractures provide critical avenues for weathering, if fracture density is lower on the south-facing slopes, then not only is there less area over which chemical weathering can occur, but also fewer opportunities for physical weathering, such as frost cracking, to affect the rock as well, thus leading to less weathered, and therefore larger, tors on the south-facing slopes.

It is difficult, however, to postulate theories of greater chemical and physical weathering occurring on the north-facing slopes from only the SHR values and fracture density measurements alone. Luckily, due in large part to the BcCZO's interest in Gordon Gulch, there have been several studies that have assessed differences in weathering processes between the north- and south-facing hillslopes in Gordon Gulch (e.g. Dethier and Lazarus, 2006; Anderson et al., 2007; Trotta, 2010; Anderson, S. et al., 2011). One such study suggests that regolith is deeper on the north-facing slope than on the south-facing slope; and that north-facing slopes have a higher moisture content and therefore likely experience more frost cracking than the south-facing slopes (Anderson, S. et al., 2011). These assessments of differences in regolith thickness, moisture, and

weathering between slopes not only support the before mentioned hypotheses for why stronger and larger tors develop on the south-facing slope, but can also further develop this study's understanding of how these processes are related to tor formation.

Weathering along fractures is not the only force governing the weathering of a tor; the removal of regolith from the system is also required to exhume the tor outcrops. When this factor is considered in the context of a thicker regolith layer on the north-facing slope, it could be postulated that thicker regolith is acting to conceal tors on the north-facing slope, giving the illusion at the surface that they are smaller. However, since the north-facing slopes are retaining greater moisture, a greater amount of weathering can occur on them. If this is then combined with a higher fracture density, which can be thought of as more area to weather, then it makes sense that the tors on the north-facing hillslope would be more eroded and thus smaller than those on the south-facing slopes.

Higher moisture content on the north-facing slopes could also influence SHR. Previous studies have shown that increased moisture content within bedrock leads to a decrease in the compressive strength of bedrock[9], both due to increased weathering but also due to the retention of water within bedrock itself (Matsukura and Tanaka, 2000; Vasarhelyi and Van, 2006). Of course, it is impossible to know if the moisture content of the tors themselves influenced the SHR values measured during the course of this study, since moisture levels of the

[9] In the laboratory, a rock's UCS can be decreased by roughly 30-50 MPa by increasing moisture content by only 1% (Vasarhelyi and Van, 2006).

sample sites were not quantified; however, it remains possible that increased weathering due to higher moisture content on the north-facing slopes is reflected in the lower SHR values measured in this study.

Ultimately, unraveling the processes that have led to stronger, larger, more abundant tors with less dense fractures surrounded by drier and shallower regolith on the south-facing slope is outside the scope of this study. However, the theories postulated here serve to better inform models of hillslope evolution and development by providing a numerical quantification of rock strength, which is an integral facet of the system.

Tor Development on Hillslopes

Tors are generally associated with decreased weathering from the top down (Linton, 1955); however, this theory is not supported by the data collected for this study. The most likely interpretation of the anomalously lower SHR values measured on the up-slope sides of tors is that the tors may behave like braking blocks when on a hillslope (Putkonen et al., 2010): accumulating regolith up-slope and allowing down slope mass movement of newly mobilized regolith away from the tor's down-slope face. If true, fresher rock with a higher SHR would be more frequently exposed on the down-slope face of tors, and weathered rock from the up-slope side of the tor, with fewer opportunities to be mobilized and transported away, would remain in place, yielding lower SHR values.

When the up-slope and down-slope strength measurements are compared between the two hillslopes, it is apparent that the down-slope faces of tors on the south-facing slope are not only stronger than the up-slope faces on that hillslope, but also stronger than both up-slope and down-slope faces on the north-facing slope (Figure 37). The similarity in strength between the up-slope and down-slope faces on the north-facing slope is probably related to the predominance of metasedimentary tors on the north-facing slope. Since the foliation of the metasedimentary rock is sub-parallel to the north-facing hillslope (Trotta, 2010), when the up-slope and down-slope faces of the metasedimentary tors are tested, both orientations will most likely be testing the same foliation plane, thus, both should yield a similar SHR value. However, this could not happen on the south-facing slope, since the foliation is sub-perpendicular to the hillslope. Previous work has related the sub-parallel relationship between foliation and the north-facing slope, along with the presence of smaller tors and a less significant slope angle, to slower local rates of erosion (Trotta, 2010). Since the south-facing slopes are steeper and have less mantled regolith, erosion rates are probably faster there than on the north-facing slope. Faster rates of erosion, coupled with the concept of a tor acting as a breaking block, could mean that part of the reason that the down-slope sides of tors on the south-facing slope are stronger is that material is being moved away from those faces much faster than anywhere else in the gulch.

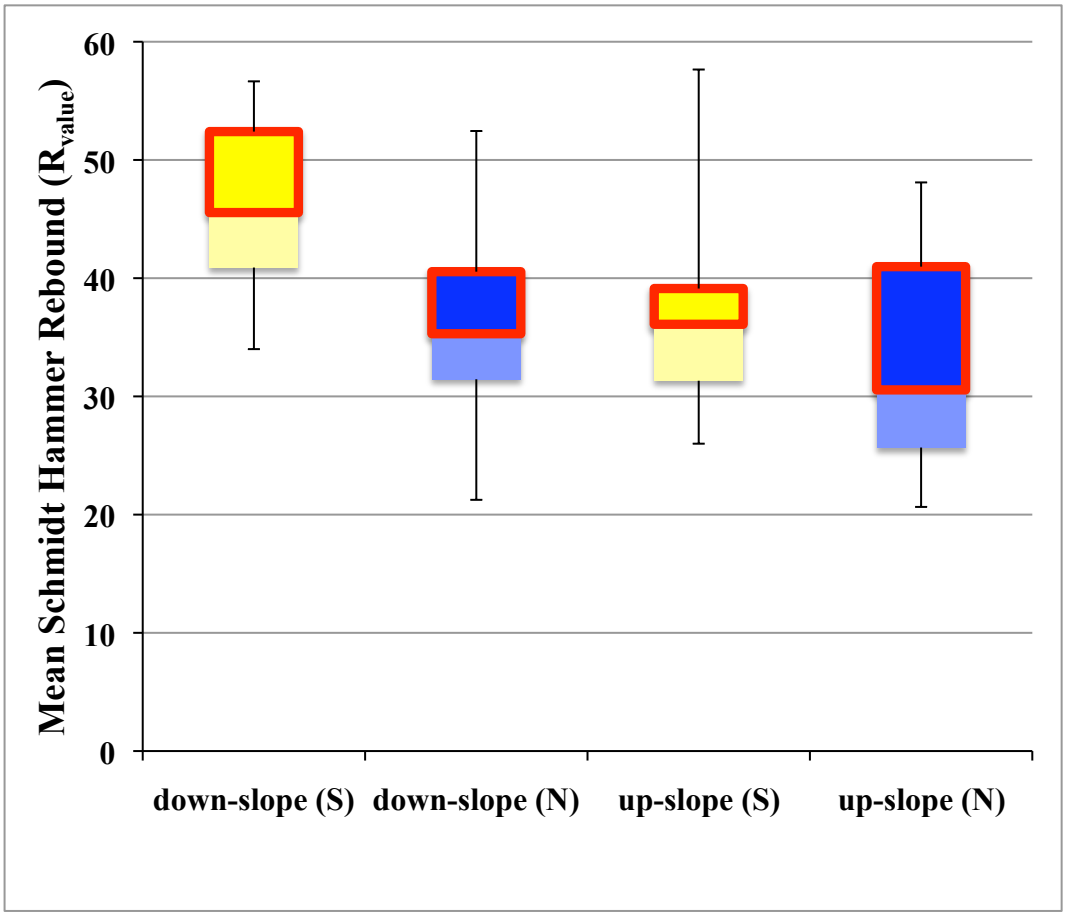

Figure 37: Mean Schmidt Hammer Rebound with respect to face orientation as well as slope aspect (N = north-facing slope, S = south-facing slope). The 3rd quartile of each data set is boxed in red. The down-slope faces of tors on the south-facing slope are the strongest, while all other face orientations on both slopes are weaker and comparable to one another.

Rock Strength Throughout the Catchment

The SHR measurements collected in this study were combined with the SHR data from an earlier study in Gordon Gulch (Dethier, 2011) to evaluate if there is a demonstrable trend in rock strength throughout the gulch (Figure 38). When this prediction map is evaluated, it is clear that outcropping bedrock in Gordon Gulch is fairly comparable in strength. However, the north-facing slopes and the bedrock in the channel below the knick point are both weaker than the majority of the outcropping bedrock. These predictions align with expectations of rock strength in this catchment since, as explained above, the tors on the north-facing slopes tend to be weaker and the bedrock below the knick point in the channel bottom should be relatively weaker as well.

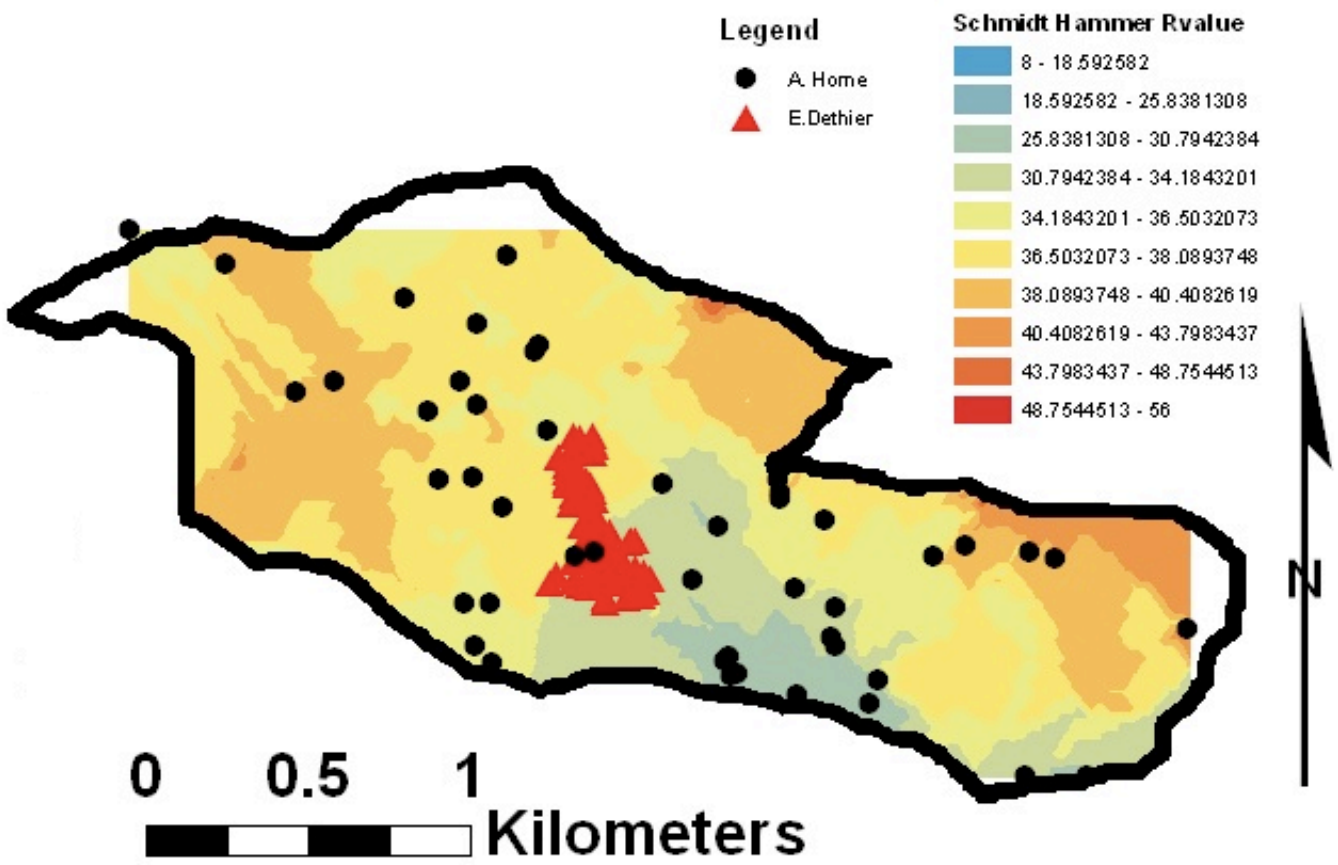

Figure 38: CoKrig image of Gordon Gulch (outlined in black) compiled from this study's data as well as the data from E. Dethier, 2011. Illustrates predicted bedrock outcrop strength throughout the gulch, which is largely homogeneous, with the exception of the north-facing slope and bedrock at the knick point in the channel that is weaker.

Study Limitations and Plans for Future Research

The conclusions reached in this study are somewhat limited by the technical aspects of sampling and data collection. Had it been known while in the field that cores of a particular size were going to be needed to test uniaxial compressive strength in the laboratory, larger samples could have been procured and more extensive laboratory testing could have been integrated into the concepts posited in this study. An incomplete understanding of testing procedure with the Schmidt Hammer also limited the reliability of the data procured. Buffing / preparing of the test surface as well as documenting the incidence angle would likely have reduced some of the noise seen in the data sets, while calibration of the device may have aligned the SHR values more closely with UCS measurements.

Future work should be directed at improving the sampling methodology in the ways stated above, but also by furthering our understanding of rock strength by studying these rocks on a much smaller scale. For example, it would be prudent to investigate if there is a mineralogical or micro-structural explanation for the variances seen in strength (e.g. between the polished and weathered alpine bedrock from Green Lakes Basin). Alternatively, a seismic refractivity study within Gordon Gulch could explore the subsurface geometry of the tors to see if the variance in size from one hillslope to another is superficial due to soil depths / coverage or if tors on the north-facing slope are smaller beneath the surface as well. Cores could also be collected from regolith mantled areas in Gordon Gulch

to investigate if tors truly did develop in areas of lower fracture density, and if so, how much more densely spaced are fractures in the saprolite by comparison to fractures in the tors. However, it would ultimately be most rewarding if a numeric quantification of rock weathering based on UCS / SHR could be incorporated into a hillslope evolution model to "describe the evolution of material within the weathered bedrock" as described by Anderson, R. et al. (2011).

CONCLUSIONS

This study has shown that rock strength decreases with increased weathering across the Boulder Creek watershed. The strongest bedrock observed was both the deepest (road cuts) and that which has maintained glacial polish. Once bedrock weathers, it weakens to an intermediate range of uniaxial compressive strength, which has been shown not only by the tors and road cuts tested in this study, but also by the weathered bedrock in Green Lakes Basin. Furthermore, with increased chemical and physical weathering, bedrock deteriorates to the weakest rock in the watershed, as demonstrated with the saprolite in both Gordon and Betasso Gulch.

This study has also found that the metasedimentary rock in the Boulder Creek watershed has a slightly higher compressive strength than the local granitic lithologies. Furthermore, the Schmidt Hammer's assessment of the metasedimentary rock is independent of the device's orientation with respect to the foliation.

In Gordon Gulch, a combination of structural anisotropy, microclimate, and regolith removal appear to be some of the dominant forces governing tor

location and size. A tor's location on a hillslope may also change the top-down weathering gradient typically associated with tors due to foliation characteristics, slope angle, and a tor's behavior similar to that of a breaking block.

In conclusion, this study has accomplished its initial goals of numerically quantifying rock strength throughout the Boulder Creek watershed and furthering our understanding of the processes affecting hillslope development in Gordon Gulch.

REFERENCES

Anderson, R., Anderson, S., & Tucker, G. (Submitted Nov, 2011). Rock Damage and the Regolith Conveyor Belt: Process Geomorphology of the Critical Zone. *Earth Surface Processes and Landforms*.

Anderson, S. P., Anderson, R. S., Hinckley, E. L. S., Kelly, P., & Blum, A. (2011). Exploring Weathering and Regolith Transport Controls on Critical Zone Developement with Moels and Natural Experiments. *Applied Geochemistry, 26* (Supplement), S3-S5.

Anderson, S. P., von Blanckenburg, F., & White, A.F. (2007). Mechanical-Chemical Interactions Shape the Critical Zone and Fluxes from it. *Elements*. *3*, 315–319.

Aydin, A., & Basu, A. (2005). The Schmidt Hammer in Rock Material Characterization. *Engineering Geology , 81*, 1-14.

Befus, K. M., Sheehan, A. F., Leopold, M., Anderson, S. P., & Anderson, R. S. (2011). Seismic Constraints on Critical Zone Architecture, Boulder Creek Watershed, Front Range, Colorado. *Vadose Zone Journal , 10* (3), 915-927.

Cole, J. C., & Braddock, W. A. (2009). *Geologic Map of the Estes Park 30′ x 60′ quadrangle, North-Central Colorado.* U.S. Geologic Survey, U.S. Department of the Interior. U.S. Geologic Survey Scientific Investigations Map 3039.

Day, M. J., & Goudie, A. S. (1977). Field Assessment of Rock Hardness Using the Schmidt Test Hammer. *British Geomorphological Research Group Technical Bulletin , 18*, 19-29.

Deere, D. U., & Miller, R. P. (1966). *Engineering Classification and Index Properties for Intact Rock.* University of Illinois. Air Force Weapons Laboratory: Research and Technology Division.

Dethier, E. (2011). *Examining Knickpoints in the Middle Boulder Creek Catchment, Colorado.* Williams College, Undergraduate Thesis.

Dethier, D. P., & Lazarus, E. D. (2006). Geomorphic Inferences from Regolith Thickness, Chemical Denudation and CRN Erosion Rates Near the Glacial Limit, Boulder Creek Catchment and Vicinity, Colorado. *Geomorphology, 75*, 384-399.

Dickinson, W.R., Klute, M.A., Hayes, M.J., Janecke, S.U., Lundin, E.R., McKittrick, M.A., Olivares, M.D. (1988). Paleogeographic and Paleotectonic Setting of Laramide Sedimentary Basins in the Central Rocky Mountain Region. *Geological Society of America Bulletin*, *100*, 1023-1039.

Dühnforth, M., & Anderson, R. S. (2011). Reconstructing the Glacial History of Green Lakes Valley, North Boulder Creek, Colorado Front Range. *Arctic, Antarctic, and Alpine Research , 43* (4), 527-542.

Ehlen, J., & Wohl, E. (2002). Joints and Landform Evolution in Bedrock Canyons. *Japenese Geomorphological Union , 23* (2), 237-255.

ELE International, Inc. *Technical Data: RM710 Rock Classification Hammer.* Loveland, CO.

Fookes, P. G., Dearman, W.R., Franklin, J.A. (1971). Some Engineering Aspects of Rock Weathering with Field Examples from Dartmoor and Elsewhere. *Quarterly Journal of Geology & Hydrogeology*, *4* (3), 139-185.

Geotechnical Control Office. (1988a). *Guide to rock and soil description, Geoguide 3.* Hong Kong Government.

Goudie, A. S. (2006). The Schmidt Hammer in Geomorphological Research. *Progress in Physical Geography, 30* (6), 703-718.

Hack, R., & Huisman, M. (2002). Estimating the Intact Rock Strength of a Rock Mass by Simple Means. In J. van Rooy, & C. Jermy (Ed.), *Engineering Geology for Developing Countries* (pp. 1971-1977). Durban, South Africa: International Association for Engineering Geology and the Environment.

Hoek, E., Marinos, P., Benissi, M. (1998). Applicability of the Geologic Strength Index (GSI) Classification for Very Weak and Sheared Rock Masses: The Case of the Athens Schist Formation. *Bull. Eng. Geol. Env.*, *57*, 151-160.

Hucka, V. (1965). A Rapid Method for Determining the Strength of Rocks In Situ. *International Journal of Rock Mechanics and Mining Science , 2*, 127-134.

Kellogg, K. S., Shroba, R. R., Bryant, B., & Premo, W. R. (2008). *Geologic Map of the Denver West 30′ x 60′ Quadrangle, North-Central Colorado: U.S. Geological Survey Scientific Investigations Map 3000, scale 1:100,000.* United States Geologic Survey, United States Department of the Interior. Reston, VA: USGS.

Li, X., Rupert, G., Summers, D., Santi, P., & Liu, D. (2000). Analysis of Impact Hammer Rebound to Estimate Rock Drillability. *Rock Mechanics and Rock Engineering , 33* (1), 1-13.

Linton, D. (1955). The Problem of Tors. *The Geographical Journal , 121* (4), 470-481+487.

Mabee, S. B., & Hardcastle, K. C. (1997). Analyzing Outcrop-Scale Fracture Features to Supplement Investigations of Bedrock Aquifers. *Hydrogeology Journal, 5* (4), 21-36.

Manda, A. K., Mabee, S. B., & Wise, D. U. (2008). Influence of Rock Fabric on Fracture Attribute Distribution and Implications for Groundwater Flow in the Nashoba Terrane, Eastern Massachusetts. *Journal of Structural Geology, 30*, 464-477.

Matsukura, Y., & Tanaka, Y. (2000). Effect of Rock Hardness and Moisture Content on Tafoni Weathering in the Granite of Mount Doeg-Sung, Korea. *Geografiska Annaler, 82* (A), 59-67.

McMillan, M. E., Heler, P. L., & Wing, S. L. (2006). History and Causes of Post-Laramide Relief in the Rocky Mountain Orogenic Plateau. *Geological Society of America Bulletin, 118* (3-4), 393-405.

Molnar, P., Anderson, R. S., & Anderson, S. P. (2007). Tectonics, Fracturing of Rock, and Erosion. *Journal of Geophysical Research , 112*.

Moore, J. R., Sanders, J. W., Dietrich, W. E., & Glaser, S. D. (2009). Influence of Rock Mass Strength on the Erosion Rate of Alpine Cliffs. *Earth Surface Processes and Landforms*, *34* (10), 1339-1352.

Nicholson, D. T. (2008). Rock Control in Microweathering of Bedrock Surfaces in a Periglacial Environment. *Geomorphology, 101*, 655-665.

Peterman, Z. E., Hedge, C.E., and Braddock, W.A. (1968). Age of Precambrian Events in the Northeastern Front Range, Colorado. *Journal of Geophysical Research*, *73* (6), 2277-2296.

Proceq. (2006). *Concrete Test Hammer: Operating Instructions*. Switzerland: Proceq SA.

Putkonen, J., Morgan, D. J., & Balco, G. (2011). Regolith Transport Quantified by Braking Block, McMurdo Dry Valleys, Antartica. *Geomorphology , http://dx.doi.org/10.1016/j.geomorph.2011.12.010.*

Sonnenbery, S. A., & Bolyard, D. W. (1997). Tectonic History of the Front Range in Colorado. In S. A. Sonnenbery, & D. W. Bolyard (Ed.), *Geologic History of the Colorado Front Range.* Denver: Rocky Mountain Association of Geologists.

Street, F. (1971). *A Study of Tors in the Front Range of the Mountains in Colorado with Special Reference Value as an Indicator of Non-Glaciation.* Cambridge, England: Cambridge University.

Trotta, J. (2010). *The Distribution of Tors in Gordon Gulch, Front Range, Colorado.* Williams College, Undergraduate Thesis.

Tucker, G. (n.d.). *Geomorphology*. Retrieved Jan 2012, from National CZO Program: Boulder Creek Critical Zone Observatory: http://czo.colorado.edu/inter/geomorphology.shtml

Tugrul, A. (2004). The Effect of Weathering on Pore Geometry and Compressive Strength of Selected Rock Types from Turkey. *Engineering Geology , 75*, 215-227.

Twidale, C. (1990). The Origin and Implications of Some Erosional Landforms. *The Journal of Geology, 98* (3), 343-364.

Vasarhelyi, B., & Van, B. (2006). Influences of Water Content on the Strength of Rock. *Engineering Geology, 84*, 70-74.

Viles, H., Goudie, A., Grab, S., & Lalley, J. (2011). The Use of the Schmidt Hammer and Equotip for Rock Hardness Assessment in Geomorphology and Heritage Science: a Comparative Analysis. *Earth Surface Processes and Landforms, 36*, 320-333.

NAME	NOTE (GP=glacial polish / WX= weathered)	LITHOLOGY	MEAN R_{VALUE}
AGL1	G.P.	Meta-Sed	63
AGL2	G.P.	Granitic	61
AGL3 (A)	G.P.	Meta-Sed	66
AGL3 (B)	G.P.	Granitic (dike)	60
AGL4	G.P.	Meta-Sed	62
AGL5	WX	Meta-Sed	23
AGL6	G.P.	Meta-Sed	60
AGL7 (A)	G.P.	Granitic (dike)	61
AGL7 (B)	WX	Granitic (dike)	42
AGL8	G.P.	Meta-Sed	57
AGL9	G.P.	Meta-Sed	56
AGL10	G.P.	Meta-Sed	60
AGL11 (A)	G.P.	Granitic (dike)	55
AGL11 (B)	G.P.	Meta-Sed	61
AGL12	G.P.	Meta-Sed	58
AGL13	G.P.	Meta-Sed	56
AGL14	G.P.	Granitic	69
AGL15	G.P.	Meta-Sed	59
AGL16	WX	Granitic	44
AGL17	hand sample collected	Meta-Sed & Granitic	-
AGL18	G.P.	Meta-Sed	46
AGL19 (A)	G.P.	Granitic	43
AGL19 (B)	WX	Granitic	23

NAME	TYPE	LITHOLOGY	Depth below surface (m)	ASPECT of Surrounding Hillslope (N Vs. S)	MEAN TOP OF TOR R-VALUE	MEAN DOWN SLOPE R-VALUE	MEAN UP SLOPE R-VALUE	MEAN R-VALUE FOR ENTIRE TOR	MEAN FRACTURE SPACING (cm)	For Metaseds: Schmidt Hammer measured parallel or perpendicular to foliation
AGG1	Tor	Meta-Sed		S	-	41	31	36	46	Perpendicular
AGG2	Tor	Meta-Sed		S	-	53	39	46	57	d=para/u=perp
AGG3	Tor	Meta-Sed		N	-	48	31	39	57	d=perp/u=para
AGG4	Tor	Meta-Sed		S	-	41	26	33	20	d=perp/u=para
AGG5	Tor	Meta-Sed		S	44	57	35	45	57	Parallel
AGG6	Tor	Meta-Sed		S	36	48	46	43	27	Perpendicular
AGG7	Tor	Meta-Sed		N	-	31	-	31	-	-
AGG8	Tor	Granitic		S	-	34	31	33	100	-
AGG9	Tor	Granitic		S	-	42	39	41	100	-
AGG10	Tor	Meta-Sed		S	-	54	48	51	50	Parallel
AGG11	Tor	Granitic		N	34	21	21	25	36	-
AGG12	Tor	Granitic		S	24	46	37	36	62	-
AGG13	Tor	Meta-Sed		S	-	38	36	37	56	d=para/u=perp
AGG14	Tor	Granitic		S	-	41	29	35	35	-
AGG15	Tor	Granitic		S	-	44	35	40	53	-
AGG16	Tor	Granitic		S	-	-	30	30	-	-
AGG17	Tor	Granitic		S	-	35	29	32	32	-
AGG18	Saprolite	Meta-Sed	0.4	S	-	-	-	43	-	-
AGG19	Saprolite	Meta-Sed	.3 / 1.2	S	-	-	-	27	-	-
AGG20	Tor	Meta-Sed		N	-	35	41	38	-	d=perp/u=para
AGG21	Tor	Meta-Sed		N	-	32	41	36	-	d=perp/u=para

AGG22	Tor	Meta-Sed		S		-	47	33	40	24	d=perp/u=para	
AGG23	Tor	Meta-Sed		S		-	41	38	40	40	Parallel	
AGG24	Tor	Granitic		S		-	54	58	56	28	-	
AGG25	Tor	Granitic		S		-	39	46	43	52	-	
AGG26	Tor	Granitic		S		-	56	30	43	46	-	
AGG27	Tor	Meta-Sed			N	48	52	44	48	59	Perpendicular	
AGG28	Tor	Meta-Sed		S		35	52	33	40	72	Perpendicular	
AGG29	Tor	Meta-Sed		S		42	46	38	42	47	Parallel	
AGG30	Tor			S		38	-	-	38	-	-	
AGG31	Tor	Meta-Sed			N	28	32	48	36	10	d=perp/u=para/t=perp	
AGG32	Tor	Meta-Sed			N	36	40	30	35	23	d=perp/u=perp/t=para	
AGG33	Saprolite	Meta-Sed	1		N	-	-	-	19	-	-	
AGG34	Tor	Granitic			N	-	41	26	36	17	-	
AGG35	Tor	Granitic			N	-	38	35	37	58	-	
AGG36	Tor	Granitic			N	-	24	25	25	45	-	
AGG37	Saprolite	Meta-Sed	1		N	-	-	-	13	-	-	
AGG38	Saprolite	Granitic	1.15	S		-	-	-	13	-	-	
AGG39	Tor	Granitic		S		45	40	-	42	29	-	
AGG40	Tor	Meta-Sed		S		44	46	50	47	45	d=para/u=perp/t=para	
AGG41	Tor	Granitic			N	-	-	24	24	-	-	
AGG42	Saprolite	Meta-Sed	0.87	S		-	-	-	9	-	-	
AGG43	Tor	Meta-Sed		S		28	55	37	40	24	d=perp/u=perp/t=para	
AGG44	Saprolite	Granitic	0.94		N	-	-	-	44	-	-	
AGG45	Tor	Granitic			N	23	-	-	23	-	-	
AGG46	Saprolite	Meta-Sed	0.59		N	-	-	-	8	-	-	

NAME	*note*	LITHOLOGY	AVERAGE R-VALUE	AVERAGE FRACTURE SPACING (cm)
AB1		Granodiorite	22	-
AB2.1	*first*	Pegmatitic Vein	51	33
AB2.2	*5m up rd*	Granodiorite	34	11
AB2.3	*another 5m up rd*	Granodiorite	14	-
AB3		Pegmatitic Vein	56	-
AB4		Granodiorite	0	14
AB5		Granodiorite	0	-
AB6		Granodiorite	12	8
AB7		Granodiorite	22	-
AB8		Granodiorite	11	6
AB9		Granodiorite	25	7
AB10		Granodiorite	32	16
AB11		Granodiorite	6	-
AB12		Granodiorite	24	7
AB13		Granodiorite	0	-
	granodiorite1	Granodiorite	32	14
AB14	*pegmatiticdike*	Granodiorite	26	-
	granodiorite2	Granodiorite	12	-
AB15		Granodiorite	0	-
AB16		Granodiorite	24	-
BUMMERS ROCK	*1*	Granodiorite	32	-
	2	Granodiorite	21	-
	3	Granodiorite	31	-
	4	Granodiorite	46	-
	5	Granodiorite	49	-

NAME	TYPE	Depth below original ground surface (m)	LITHOLOGY	AVERAGE R-VALUE
AR1	top	0	Granitic	45
	middle	3.1		39
	bottom	6.4		61
AR2	top	0	MetaSed: Gneiss	14
	middle	2.9		46
	bottom	8.3		53
AR3	top	0	MetaSed: Schist	19
	middle	3.3		31
	bottom	6.3		40